



Published in final edited form as:

Cell Rep. 2019 January 15; 26(3): 670–688.e6. doi:10.1016/j.celrep.2018.12.079.

The Septate Junction Protein Tsp2A Restricts Intestinal Stem Cell Activity via Endocytic Regulation of aPKC and Hippo Signaling

Chiwei Xu¹, Hong-Wen Tang¹, Ruei-Jiun Hung¹, Yanhui Hu¹, Xiaochun Ni¹, Benjamin E. Housden¹, and Norbert Perrimon^{1,2,3,*}

¹Department of Genetics, Harvard Medical School, 77 Avenue Louis Pasteur, Boston, MA 02115, USA

²Howard Hughes Medical Institute, Harvard Medical School, 77 Avenue Louis Pasteur, Boston, MA 02115, USA

³Lead Contact

SUMMARY

Hippo signaling and the activity of its transcriptional coactivator, Yorkie (Yki), are conserved and crucial regulators of tissue homeostasis. In the *Drosophila* midgut, after tissue damage, Yki activity increases to stimulate stem cell proliferation, but how Yki activity is turned off once the tissue is repaired is unknown. From an RNAi screen, we identified the septate junction (SJ) protein tetraspanin 2A (Tsp2A) as a tumor suppressor. Tsp2A undergoes internalization to facilitate the endocytic degradation of atypical protein kinase C (aPKC), a negative regulator of Hippo signaling. In the *Drosophila* midgut epithelium, adherens junctions (AJs) and SJs are prominent in intestinal stem cells or enteroblasts (ISCs or EBs) and enterocytes (ECs), respectively. We show that when ISCs differentiate toward ECs, Tsp2A is produced, participates in SJ assembly, and turns off aPKC and Yki-JAK-Stat activity. Altogether, our study uncovers a mechanism allowing the midgut to restore Hippo signaling and restrict proliferation once tissue repair is accomplished.

Graphical Abstract

This is an open access article under the CC BY-NC-ND license (<http://creativecommons.org/licenses/by-nc-nd/4.0/>).

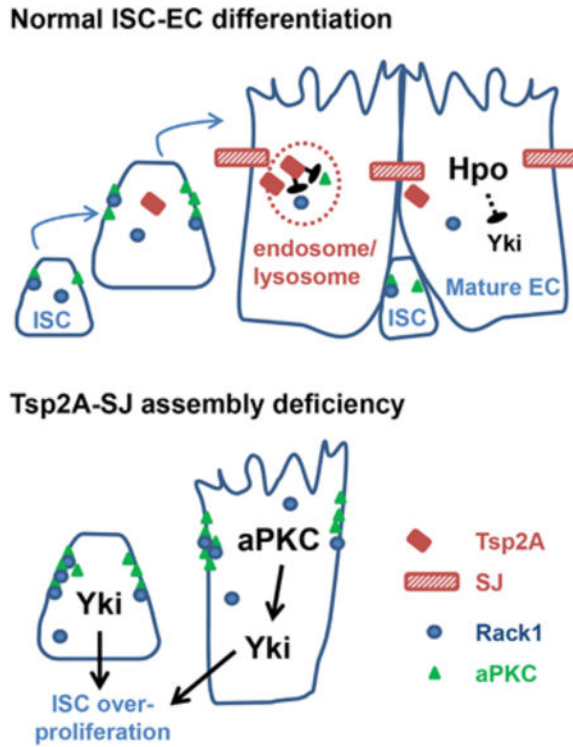
*Correspondence: perrimon@receptor.med.harvard.edu.

AUTHOR CONTRIBUTIONS

C.X. and N.P. conceived the project, interpreted the data, and wrote the manuscript. C.X. performed the experiments. H.-W.T. performed coIP experiments. R.-J.H. performed the single-cell RNA-seq and data analysis. Y.H. helped with the bioinformatics analysis of single-cell RNA-seq and tetraspanin family proteins. X.N. established the fly gut TRAP protocol. B.E.H. provided instructions for the design of sgRNA and the use of CRISPR/Cas9 technology.

DECLARATION OF INTERESTS

The authors declare no competing interests.



In Brief

SJ assembly is a hallmark of EC differentiation in the *Drosophila* midgut. Xu et al. identify SJ proteins as potent tumor suppressors and uncover Hippo signaling as the surveillance mechanism for SJ deficiency. Specifically, they demonstrate that SJ protein Tsp2A facilitates the endocytic degradation of the Hippo-pathway-antagonizing molecule aPKC.

INTRODUCTION

Precise regulation of stem cell activity is crucial for tissue turnover and necessary to prevent hyperplasia. The digestive epithelium is an excellent system to study the activity of stem cells and how their proliferation and differentiation are regulated, especially in the context of damage. In the intestine, intestinal stem cells (ISCs) give rise to new ISCs and daughter cells known as enteroblasts (EBs), which are primed for differentiation toward either absorptive ECs (~90%) or secretory enteroendocrine cells (EEs; ~10%), depending on the activity of Notch signaling (He et al., 2018; Micchelli and Perrimon, 2006; Ohlstein and Spradling, 2006). Strikingly, ISCs/EBs dramatically accelerate proliferation and differentiation in order to replenish lost cells when tissue damage causes massive EC death (Amcheslavsky et al., 2009). A number of studies have demonstrated the conserved roles of core pathways, such as epidermal growth factor receptor (EGFR)-Ras-mitogen-activated protein kinase (MAPK) signaling (Jiang et al., 2011; Powell et al., 2012), Janus kinase signal transducer and activator of transcription (JAK-Stat) signaling (Grivennikov et al., 2009; Jiang et al., 2009), and Hippo signaling (Cai et al., 2010; Karpowicz et al., 2010; Ren et al., 2010; Shaw et al., 2010), in regulating ISCs. Although the role of these pathways in proliferation and

differentiation of ISCs/ EBs has been characterized, less is known about the signals modulating their activities.

The Hippo signaling pathway is particularly essential for tissue homeostasis and cancer prevention. The core components of the Hippo pathway are conserved from *Drosophila* to mammals. In *Drosophila*, the kinase Hippo (Hpo) phosphorylates and activates the kinase Warts (Wts), with the aid of the scaffold proteins Mob as tumor suppressor (Mats) and Salvador (Sav). Activated Wts phosphorylates Yki, resulting in the cytoplasmic retention and inhibition of Yki. The mammalian Hippo network is similar but more complex, with two Hpo orthologs (MST1/2), two Wts orthologs (LATS1 or LATS2), two Mats orthologs (MOB1A or MOB1B), one Sav ortholog (SAV1), and two Yki orthologs (YAP or TAZ). When Hippo signaling is inhibited, Yki or YAP or TAZ is activated and induces transcriptional programs promoting tissue growth and inhibiting cell death (Hong and Guan, 2012; Huang et al., 2005; Zhao et al., 2008). In the digestive epithelium of both *Drosophila* (Karpowicz et al., 2010; Ren et al., 2010; Shaw et al., 2010) and mice (Cai et al., 2010; Gregorieff et al., 2015), the activity of Yki or YAP is induced to facilitate accelerated ISC proliferation following tissue damage. However, it is unclear how Yki or YAP activity is downregulated when tissue repair is complete.

Many components of the Hippo pathway are localized near cell junctions, and their activities are regulated by subcellular localization (Sun and Irvine, 2016). Most notably, recruitment of Hpo to the subapical region close to adherens junctions (AJs) by Expanded (Ex), Merlin (Mer), and Kibra facilitates Hpo dimerization and activation (Deng et al., 2013). Moreover, the cell polarity determinant protein atypical protein kinase C (aPKC) antagonizes Hippo signaling by causing Hpo delocalization from the membrane and subsequent Hpo inactivation in both *Drosophila* and mammals (Archibald et al., 2015; Grzeschik et al., 2010). Interestingly, junction proteins often exhibit differential expression between stem cells and their differentiated progenies. For example, AJs are enriched among *Drosophila* ISCs/ EBs (Choi et al., 2011; Ohlstein and Spradling, 2006), *Drosophila* germline stem cells (Song et al., 2002), mouse hematopoietic stem cells (Zhang et al., 2003), and mammalian epidermal basal or stem cells (Green et al., 2010). In contrast, septate junctions (SJs) are mainly distributed between ECs in the *Drosophila* midgut (Resnik-Docampo et al., 2017), and tight junctions (TJs; analogous to *Drosophila* SJs) are localized between differentiated epithelial cell types in the mouse epidermis (Green et al., 2010) and trachea (Gao et al., 2015). Therefore, the AJ-SJ transition and *de novo* production of SJs might provide a pivotal link between Hippo signaling and stem cell differentiation.

In an RNAi screen to interrogate the function of transmembrane proteins in ISCs/EBs, we identified the SJ protein tetraspanin 2A (Tsp2A) as a tumor suppressor. Further characterization reveals that *Tsp2A* expression initiates in ISCs and Tsp2A protein assembles at the SJs in the progenitor cells that are differentiating toward ECs. Importantly, we found that Tsp2A undergoes active internalization from the SJs and mediates the degradation of the Hippo-antagonizing protein aPKC. Therefore, endocytic regulation by Tsp2A couples the process of EC maturation with the downregulation of Yki activity. Tsp2A belongs to the large family of four-pass transmembrane proteins that often function as scaffolding co-receptors. Similar to our observation with Tsp2A, previous studies have

documented the endocytosis of a putative Tsp2A ortholog CD81 and claudins (TJ proteins) (Farquhar et al., 2012; Matsuda et al., 2004). While the internalization of Tsp2A ortholog and claudins has long been an intriguing observation in cultured cells, our finding about the Tsp2A-aPKC signaling uncovers a physiological function for the internalization of occluding junction (SJ or TJ) protein *in vivo*.

RESULTS

Tsp2A Acts as a Tumor Suppressor in the ISC-EC Lineage

Expression of *Tsp2A* RNAi (target region shown in Figure S1A; knockdown efficiency shown in Figure S1B) in ISCs and EBs using the *esgGal4 UAS-GFP tubGal80^S (EGT)* driver (Micchelli and Perrimon, 2006) causes severe hyperplasia; the midgut appears swollen, especially in the posterior region (Figures 1A and 1B), ISCs/EBs undergo massive expansion and overproliferation (Figures 1C and 1D), and the pseudostratified midgut epithelium becomes multilayered (Figures 1C' and 1D'). A detailed time course analysis suggests that overproliferation starts when *Tsp2A* RNAi is expressed in ISCs/EBs for 3 days; *Tsp2A* RNAi expression in ISCs/EBs for 5 days or longer causes a significant induction of mitosis in the midgut (Figure 1E). Mosaic analysis with a repressible cell marker (MARCM) clones generated from ISCs expressing *Tsp2A* RNAi can grow much larger than control clones expressing *Luc* RNAi (Figures 3J and 3K), suggesting that *Tsp2A* is required within the lineage of an individual ISC to restrict its clonal expansion. In addition, RNAi lines targeting different regions of the *Tsp2A* transcript (Figure S1A) consistently cause a phenotype of midgut overproliferation (Figures 1F and S3F). Moreover, the RNAi line targeting the *Tsp2A* 3' UTR can be rescued by the co-expression of *Tsp2A* cDNA in ISCs/EBs (Figures 1G–1I). Consistent with the RNAi phenotype, a pair of short guide RNAs (sgRNAs) targeting *Tsp2A* (region shown in Figure S1A) causes massive overproliferation and midgut hyperplasia when *Cas9* is expressed in ISCs/EBs (Figures 1J–1L, 1J', and 1K'). On the contrary to *Tsp2A* RNAi, expression of *Tsp2A* cDNA in ISCs/EBs (Figure S1C) causes moderate reduction of tissue damage-induced proliferation (Figure 1M).

Tsp2A is a SJ protein required for SJ assembly in the larval midgut (Izumi et al., 2016). A recent study found that depletion of the tricellular junction (TCJ) protein Gliotactin (Gli) impairs the intestinal barrier and causes infection-related c-Jun N-terminal kinase (JNK)-dependent induction of ISC proliferation in old flies (Resnik-Docampo et al., 2017). Because TCJ proteins might participate in SJ assembly, we asked whether *Tsp2A* RNAi-induced overproliferation is due to similar stress signaling. Strikingly, inhibition of JNK signaling by knocking down the kinase *basket* (*bsk*) or expressing a dominant-negative form of *bsk* (*bsk^{DN}*) cannot rescue the overproliferation phenotype caused by *Tsp2A* RNAi expression in ISCs/EBs (Figures S1D–S1H). In order to determine whether *Tsp2A* RNAi-induced overproliferation is a compensatory response to tissue damage, we stained the midguts for the apoptosis marker cleaved caspase-3 and detected minimal signs of cell death when there was apparent overproliferation following *Tsp2A* knockdown (Figures S1I–S1K). Therefore, unlike the case with *Gli* knockdown during aging, the *Tsp2A* knockdown phenotype is not caused by JNK stress signaling or tissue damage.

We further characterized the *Tsp2A* knockdown phenotype in different cell types of the midgut. Expression of *Tsp2A* RNAi in EBs with the *Su(H)Gbe-Gal4, UAS-CD8-GFP; tubGal80^{ts} (SGT)* driver (Zeng et al., 2010) (Figures S1L–S1N) or in ECs with *Myo1A^{ts}* (Figures S1O–S1Q) can induce overproliferation in the midgut, suggesting a non-autonomous effect. As it is the case with *Tsp2A* knockdown in ISCs/EBs, the *Tsp2A* knockdown phenotype in ECs can be rescued by an RNAi-resistant *Tsp2A* cDNA (Figure S1Q), but not by inhibition of JNK-mediated stress signaling with *bsk* RNAi (Figure S1R) or dominant-negative *bsk* (data not shown). Moreover, *Tsp2A* knockdown in ISCs with *DlGal4^{ts}* also causes mild overproliferation (Figure S1S). In contrast, *Tsp2A* knockdown in EEs or visceral muscles does not affect proliferation (Figure S1S). Therefore, *Tsp2A* functions as a tumor suppressor in the ISC-EC lineage.

Characterization of *Tsp2A* Expression in the ISC-EC Lineage

For a comprehensive understanding of *Tsp2A* expression, we analyzed our adult midgut single-cell RNA sequencing (RNA-seq) data (Hung et al., 2018) and reconstructed the differentiation trajectories (Figure 2A) from the transcriptomes of 1,753 cells using the single-cell trajectories reconstruction, expression, and mapping (STREAM) method, which can disentangle and visualize complex branching trajectories from single-cell transcriptomic data without prior knowledge about the structure or the number of trajectories (Chen et al., 2018). As expected, the ISC-EC differentiation trajectory is characterized by the gradual loss of ISC markers such as *headcase (hdc)* (Resende et al., 2017) (Figure 2B) and the incremental expression of EC markers such as λ -*Trypsin* (Figure 2C). Moreover, as indicated in the 2D stream plots, the expression of *shotgun*, which encodes *Drosophila* AJ protein E-cadherin, is enriched in the ISCs/EBs and decreases when ISCs differentiate toward ECs (Figure 2D). In contrast, the expression levels of *Tsp2A* (Figure 2E) and other SJ protein-coding genes (Hung et al., 2018) gradually increase during ISC-EC differentiation. Consistent with the single-cell ISC-EC trajectory reconstruction, the ultrastructural analysis with transmission electron microscopy (TEM) captures the AJ-SJ transition in a differentiating progenitor cell that partially resembles an ISC/EB (small size, dense cytoplasm, and AJ connection to the neighboring ISC/EB) and partially resembles an EC (relatively more apical localization and microvilli formation at the apical surface) (Figures S2A–S2C). The mixed properties of ISCs and ECs indicate an intermediate status, which we refer to as premature EC (pre-EC). In summary, *Tsp2A* expression and SJ formation occur during ISC-EC differentiation and precede the complete maturation of ECs.

The single-cell RNA-seq data allow us to perform co-expression analysis of *Tsp2A* with different cell-type markers and detect *Tsp2A* expression in ISCs/EBs (Figure 2F; Table S1). Whereas only a few *Dl+* ISCs are expressing *Tsp2A*, a higher percentage of *Tsp2A+* cells are detected among the cells expressing the EB marker *klumpfuss (klu)* (Hung et al., 2018). The *Tsp2A+* cell percentage and average *Tsp2A* expression levels rise even higher among cells expressing the EC markers (*Myo1A*, β -*Trypsin*, and λ -*Trypsin*). Consistent with the single-cell analysis, our recent gene-expression profiling by targeted DamID detects a low level (0.74) of *Tsp2A* expression in *esg+* cells and a high level (2.29) of *Tsp2A* expression in *Myo1A+* cells (Doupe et al., 2018). In addition, a dramatic induction of *Tsp2A* mRNA levels is detected in ISCs/EBs by translating ribosome affinity purification (TRAP) (Thomas

et al., 2012) and qRT-PCR quantification (Figures S2D–S2F) at very early stages following bleomycin feeding, which can stimulate ISC differentiation toward ECs (Amcheslavsky et al., 2009). Therefore, we conclude that *Tsp2A* expression initiates in ISCs and increases during ISC-EC differentiation.

To confirm Tsp2A protein expression and localization in EBs, we co-stained the midgut for Tsp2A and the Notch pathway activity reporter or EB marker Su(H)Gbe-GFP, which indicates the differentiation of midgut progenitor cells, especially toward ECs (Ohlstein and Spradling, 2007). Despite being expressed in a small number of cells under tissue homeostasis conditions, Su(H)Gbe-GFP labels EBs in a wide range of shapes with different levels of membrane-localized Tsp2A (Figures 2G–2I and 2G'–2I'). After bleomycin-induced tissue damage, ISC differentiation is accelerated, resulting in a greater number of Su(H) Gbe-GFP+ cells with Tsp2A assembly along the cell border (Figures 2J and 2J'). Furthermore, *Tsp2A* RNAi expression in EBs reduces the overall staining of Tsp2A in the midgut (Figures 2K, 2L, 2K', and 2L'). Therefore, Tsp2A protein is produced in EBs and assembled at SJs during ISC-EC differentiation.

Under tissue homeostasis conditions, Tsp2A staining is mostly observed in ECs and rarely in ISCs/EBs (Figures 2G–2I and S2G). However, when tissue damage induces ISC-EC differentiation, we could observe weak Tsp2A staining along cell borders of pre-ECs (as judged from their increased cell size) that retain *EGT*-driven GFP expression (Figure S2H). To investigate whether the overall staining of Tsp2A in the midgut depends on the regenerative activity of ISCs/EBs, we used *EGT*-driven *reaper* (*rpr*) expression to deplete ISCs/EBs (Figures S2I–S2M) and stained midguts for Tsp2A at different stages of tissue regeneration. The flies were fed bleomycin-containing food to cause midgut damage and returned to normal food for recovery. Strikingly, Tsp2A staining is disrupted by tissue damage but completely restored after tissue repair in the normal midgut with ISCs/EBs (Figures S2N–S2P). The post-damage recovery of Tsp2A staining is suppressed by ISC/EB depletion (Figures S2Q–S2S), highlighting the importance of ISC activity to regenerate mature ECs for the recovery of Tsp2A staining patterns following tissue damage.

***Tsp2A* Knockdown Causes the Accumulation of ISCs/EBs and Pre-ECs**

To further investigate how *Tsp2A* knockdown affects ISC differentiation, we stained the midgut for different cell-type markers. *Tsp2A* RNAi expression in ISCs/EBs induces the ISC marker *Dl-lacZ* (Figures 3A–3C) and the EB marker Su(H)Gbe-GFP (Figures 3D and 3E). By contrast, *Tsp2A* knockdown does not affect the EE marker *Pros* (Figures 3F and 3G). Interestingly, *Tsp2A* RNAi expression in ISCs/EBs results in an increased number of pre-ECs that express the EC marker *Pdm1* and retain some ISC/EB features (small nucleus or *EGT*> GFP expression) (Figures 3H and 3I). Similarly, *Tsp2A* RNAi expression induces the accumulation of *Pdm1*+ small nuclei pre-ECs in MARCM clones (Figures 3J and 3K). qRT-PCR quantification further demonstrates the induction of *Dl* and *Pdm1*, but not *Pros*, in the midgut following *Tsp2A* knockdown (Figure 3L). Therefore, *Tsp2A* knockdown induces ISC/EB expansion and ISC-EC differentiation.

Despite the induction of Su(H)Gbe-GFP and *Pdm1*, *Tsp2A* knockdown causes dramatically reduced expression of genes encoding trypsins (e.g., β -*Trypsin* and ϵ -*Trypsin*) in the midgut

(Figure 3L), suggesting a lack of functional ECs. Furthermore, the ultrastructural analysis by TEM suggests that *Tsp2A* knockdown not only transforms the pseudostratified midgut epithelium into multilayers but also causes microvilli formation in many pre-ECs that maintain ISC/EB-like features (i.e., basal localization, small nucleus, and dense cytoplasm) (Figures 3M–3O). In conclusion, ISCs/EBs expressing *Tsp2A* RNAi cannot fully differentiate into mature ECs.

SJ Proteins Form an Interdependent Network Distinct from Other Junctions in the Midgut

Different types of junction proteins often depend on each other for their localization and function. For example, in *Drosophila* embryonic epithelia, the basolateral junction (BLJ) proteins are interdependent (Bilder et al., 2000) and required for the junctional localization of AJs (Bilder and Perrimon, 2000). We examined in the midgut whether the depletion of the SJ protein *Tsp2A* affects the localization of other junction proteins. Strikingly, whereas *Tsp2A* knockdown (Figures 4A and 4B) causes defects in junctional localization of other SJ proteins, such as Mesh, Snakeskin (*Ssk*), and Coracle (*Cora*) (Figures 4C–4H), it induces the expression of the AJ protein Armadillo (*Arm*) (Figures 4I and 4J) or the BLJ protein Lethal giant larvae (*Lgl*) (Figures 4K and 4L). For the ultrastructural analysis of how *Tsp2A* knockdown affects cell junctions, we obtained electron micrographs and found that junctions are weakened but still present between ECs in midguts ubiquitously expressing *Tsp2A* RNAi (Figures 4M–4P). Moreover, as other non-SJ junction proteins are probably still present, blue dye fed to young adult flies (in the “Smurf assay”; Rera et al., 2012) expressing *Tsp2A* RNAi in ISCs/EBs or ubiquitously does not leak out of the guts (Figures 4Q and 4R), suggesting a functional intestinal barrier. Interestingly, a recent study found that the AJ protein E-cadherin is also dispensable for barrier function (Liang et al., 2017). Therefore, different junctions might function in a redundant manner to control the transepithelial permeability of the midgut in young adult flies.

Next, we asked whether knockdown of other junction proteins affects *Tsp2A* localization. In addition to previous findings that Mesh and *Ssk* are required for *Tsp2A* assembly at SJs (Izumi et al., 2016), depletion of another SJ protein, *Cora*, but not *Arm* or *Lgl*, disrupts *Tsp2A* localization (Figures 4S–4X). Furthermore, we compared the localization of different junction proteins before and after tissue damage. After bleomycin feeding for 2 days, overall Mesh staining is disrupted and reduced in the midgut (Figures S3A and S3B), which is reminiscent of *Tsp2A*. In contrast, the expression of *Arm* increases among the expanding population of progenitor cells after tissue damage (Figures S3C and S3D). In summary, whereas SJ proteins (*Tsp2A*, Mesh, *Ssk*, *Cora*) depend on each other for junctional localization, *Tsp2A* does not appear to depend on or determine the membrane recruitment of other types of junctions in the midgut.

We further analyzed the knockdown of different junction proteins and compared their effects on ISC activity. Knockdown of different SJ genes (*Tsp2A*, *Mesh*, *Ssk*, and *cora*) causes a similar extent of ISC/EB expansion (Figures S3E–S3K). In contrast, knockdown of *arm* or *Lgl* in ISCs/EBs does not cause an easily discernible phenotype (Figures S3L–S3O), except that ISCs/EBs expressing *Lgl RNAi* exhibit enhanced regenerative proliferation after tissue damage (Figure S3O). Moreover, *Gli* knockdown does not affect midgut proliferation under

either homeostatic or tissue damage conditions in young adult flies (Figures S3P–S3V). Therefore, the interdependent network of SJ proteins functions as a critical tumor suppressor in the midgut, which is different from other types of junction proteins such as Arm, Lgl, and Gli.

Tsp2A Participates in Endocytic Regulation

A detailed characterization of Tsp2A expression in the midgut reveals a striking pattern of subcellular localization in various intracellular punctae, in addition to the expected localization at SJs, in EBs and ECs (Figures 2I', 2J', 5A, and 5B). These Tsp2A punctae, when visualized by GFP-Tsp2A expression, appear to correspond to acidic compartments based on LysoTracker staining (Figure 5C). In addition, the endocytosis assay (Shravage et al., 2013) suggests that some Tsp2A punctae co-localize with internalized Texas-red-labeled avidin particles (Figure 5D). Moreover, these Tsp2A punctae also partially co-localize with the early endosome marker Hrs and the late endosome marker Rab7 (Riedel et al., 2016) (Figures 5E and 5F). Furthermore, TEM with immunogold labeling demonstrates the localization of GFP-Tsp2A at endosomes and lysosomes, in addition to the expected localization at SJs (Figures 5G–5I). Therefore, we propose that Tsp2A undergoes active internalization and endocytic degradation.

Next, we asked how Tsp2A expression is affected when different steps of the endocytic pathway are inhibited by manipulating different GTPases (Zhang et al., 2007). Inhibition of endocytosis (internalization from the plasma membrane) by *Rab5* knockdown causes Tsp2A aggregation at the cell surface and a decrease in the number of intracellular Tsp2A punctae, whereas inhibition of endosome recycling by *Rab11* knockdown causes Tsp2A accumulation in the intracellular punctae (Figures 5J–5O and 5J'–5O', phenotype observed mostly in pre-ECs and ECs as judged from the size of their nuclei; quantification shown in Figure 5P). Consistent with the RNAi phenotype, the dominant-negative form of *Rab5* (*Rab5^{DN}*) or *Rab11* (*Rab11^{DN}*) causes the accumulation of Tsp2A staining at the cell surface or in the intracellular punctae, respectively (Figures S4A–S4F and S4A'–S4F'). Altogether, our data support the hypothesis that Tsp2A participates in the endocytic pathway.

Similar to *Tsp2A* knockdown, the expression of *Rab5* RNAi or *Rab5^{DN}* in ISCs/EBs causes dramatic midgut overproliferation, whereas the dominant-negative forms or RNAi lines of *Rab7* (controlling endosome maturation) and *Rab11* have much less or no influence on proliferation (Figures S4G–S4L). In contrast to the *Rab5* loss-of-function phenotype, forcing endocytosis with the constitutively active form of *Rab5* (*Rab5^{ca}*) in ISCs/EBs inhibits proliferation (Figures S4M–S4Q). Moreover, the overproliferation phenotype caused by *Tsp2A* RNAi expression in ISCs/EBs can be rescued by *Rab5^{ca}* rather than the constitutively active form of *Rab7* (*Rab7^{ca}*) or *Rab11* (*Rab11^{ca}*) (Figures S4R–S4V). In addition, the co-expression of *Rab5^{ca}* in ECs can suppress the overproliferation phenotype caused by *Myo1A^{ts}*-driven *Tsp2A* RNAi expression (Figure S4W). Therefore, the role of Tsp2A as a tumor suppressor in the ISC-EC lineage might be related to the endocytosis process that implicates Tsp2A.

aPKC-Yki-JAK-Stat Mediates the Overproliferation Phenotype Caused by *Tsp2A* Knockdown

Although *Tsp2A* RNAi-induced overproliferation appears similar to the phenotype caused by *Rab5* RNAi or *Rab5^{DN}*, *Tsp2A* knockdown does not cause the overall elimination of early or late endosomes (Figures 5Q–5T). Therefore, the role of *Tsp2A* as a tumor suppressor could not simply be attributed to the broad inhibition of endocytosis. To identify the specific downstream signaling events regulated by *Tsp2A* and required for *Tsp2A* RNAi-induced overproliferation, we performed a suppressor screen among proteins that interact with *Tsp2A* or its putative orthologs (BioGRID; <https://thebiogrid.org>) (Table S2). Multiple different RNAi reagents targeting *aPKC* or its co-factor, *Receptor of activated protein C kinase 1* (*Rack1*), inhibit *Tsp2A* RNAi-induced overproliferation (Figures 6A–6D and 6I; knockdown efficiency shown in Figures S5A and S5B). When expressed alone in ISCs/EBs, *aPKC* RNAi (using the reagent causing weak knockdown) or *Rack1* RNAi cannot block tissue-damage-induced mitosis, whereas strong knockdown of *aPKC* completely inhibits mitosis (Figure S5C), suggesting that a minimal level of aPKC is required for proliferation. We further analyzed aPKC function in different cell types. Consistent with the observation in ISCs/EBs, *aPKC* knockdown in EBs moderately suppresses tissue-damage-induced proliferation (Figure S5D). Moreover, *aPKC* RNAi also suppresses the overproliferation phenotype caused by *Myo1A^{ts}*-driven *Tsp2A* RNAi expression in ECs (Figure S5E). Therefore, aPKC activity is required for the *Tsp2A* knockdown phenotype in the ISC-EC lineage.

Knockdown of most candidates identified from the suppressor screen, such as *myspheroid* (*mys*, *Drosophila* ortholog of β integrin), *Akt1*, or *EGFR*, not only rescue *Tsp2A* RNAi-induced overproliferation, but also completely block ISC regenerative proliferation (Table S2). Although tetraspanins are often associated with integrins to modulate integrin-dependent cell adhesion and migration (Hemler, 2005), it is difficult to attribute the *Tsp2A* knockdown phenotype to integrin signaling, since *mys* is generally required for ISC proliferation (Lin et al., 2013), and we did not detect abnormal *mys* staining following *Tsp2A* knockdown in the midgut (data not shown). Similarly, *Akt1* and *EGFR* are known as essential genes for ISC maintenance and proliferation (Jiang and Edgar, 2011). In contrast, ISCs/EBs expressing *Tsp2A* RNAi together with *aPKC* RNAi (the weak reagent) or *Rack1* RNAi can still exhibit regenerative proliferation following tissue damage (Figures 6E–6I). Therefore, we focused on aPKC or *Rack1* in pursuit of a mechanistic understanding about how *Tsp2A* knockdown affects proliferation.

Previous studies have suggested that aPKC induces Yki activity in the eye imaginal discs (Grzeschik et al., 2010). To examine whether aPKC also antagonizes Hippo signaling and activates Yki in the midgut, we expressed a constitutively active, N-terminally truncated form of aPKC (*aPKC^N*) (Betschinger et al., 2003) in ISCs/EBs and stained for the Yki activity reporter *Diap1-lacZ*. The results suggest that *aPKC^N* causes ISC/EB expansion and Yki activation (Figures 6J and 6K). Consistent with the previous findings that Yki acts both autonomously in ISCs/EBs and non-autonomously in ECs to induce midgut proliferation (Karpowicz et al., 2010; Ren et al., 2010; Shaw et al., 2010), *aPKC^N* expression in ECs also stimulates proliferation (Figure S5F). Furthermore, the overproliferation phenotype

caused by the expression of constitutively active *Yki* (*Yki^{3SA}*) in ISCs/EBs cannot be suppressed by *aPKC* RNAi or *Rack1* RNAi (Figure S5G). In conclusion, aPKC or Rack1 regulates midgut proliferation via Yki activity.

To examine whether *Tsp2A* knockdown activates Yki, we stained midguts with two different Yki reporters (*Diap1-lacZ* and anti-Ex antibody; Maitra et al., 2006) and observed dramatically induced Yki activity in ISCs/EBs expressing *Tsp2A* RNAi (Figures 6L–6O). qRT-PCR confirmed that mRNA levels of *Diap1*, *upd3*, and *ImpL2*, all induced by Yki activation (Karpowicz et al., 2010; Kwon et al., 2015), increase in midguts expressing *Tsp2A* RNAi in ISCs/EBs (Figure 6P). Consistent with the induction of the JAK-Stat pathway ligand *upd3*, the reporter for JAK-Stat activity is induced following *Tsp2A* knockdown (Figures 6Q and 6R). Moreover, electron micrographs reveal the ultrastructural similarity between Yki activation and *Tsp2A* knockdown; the midgut epithelium expressing *Yki^{3SA}* in ISCs/EBs becomes multilayered and forms microvilli in the pre-ECs that have not yet reached the lumen (Figures S5H–S5J). Furthermore, we compared the kinetics of Yki activity to *Tsp2A*-SJ assembly at different stages of tissue damage or repair by staining the midguts with the anti-Ex antibody. Consistent with the previous report (Karpowicz et al., 2010), Yki activity is induced in the expanding population of progenitor cells after tissue damage and downregulated to the normal levels after tissue repair (Figures S5K–S5M). Altogether, Yki activity is induced by *Tsp2A* knockdown and appears to inversely correlate with the kinetics of *Tsp2A*-SJ assembly following tissue damage.

To determine whether Yki activation or Hippo inhibition is required for *Tsp2A* RNAi-induced overproliferation, we expressed *Yki* RNAi or *hpo* cDNA together with *Tsp2A* RNAi in ISCs/EBs and found that both can rescue the overproliferation phenotype (Figures 6S, 6T, and 6W–6Z). Consistent with the previous findings that Yki depends on JAK-Stat activation to induce overproliferation (Karpowicz et al., 2010; Ren et al., 2010; Staley and Irvine, 2010), knockdown of JAK-Stat pathway components (*dome*, *Stat92E*, and *hop*) can rescue *Tsp2A* RNAi-induced overproliferation (Figures 6U, 6V, and 6Y; Table S2). Moreover, reduction of JAK-Stat activity by replacing one copy of wild-type *hop* with the amorphic allele (*hop²* or *hop²⁷*) not only rescues the *Tsp2A* knockdown phenotype but also allows ISCs expressing *Tsp2A* RNAi to respond to tissue damage by induced proliferation (Figure S5N). In summary, aPKC-Yki-JAK-Stat signaling mediates *Tsp2A* RNAi-induced overproliferation.

Tsp2A Interacts with aPKC or Rack1 to Mediate Their Endocytic Degradation

We further investigated the mechanism by which *Tsp2A* regulates aPKC and Rack1. The mammalian orthologs of *Tsp2A* are known to interact with protein kinase C and Rack1 (Perez-Hernandez et al., 2013; Zhang et al., 2001); whereas Rack1 is supposed to bind and stabilize activated protein kinase C (Vani et al., 1997). We confirmed the *Tsp2A*-aPKC and *Tsp2A*-Rack1 interactions (Figures 7A and 7B), as well as an interaction between aPKC and Rack1 (Figures S6A and S6B), by co-immunoprecipitation (coIP) experiments in *Drosophila* S2R+ cells. When hemagglutinin (HA)-tagged *aPKC-HA* or *Rack1-HA* is ubiquitously expressed in the midgut, its signals can be found concentrated at intracellular *Tsp2A* punctae (Figures 7C and 7D). Although endogenous aPKC staining signals are rare, we also

observed its co-localization with the Tsp2A punctae visualized by FLAG-HA-tagged FH-Tsp2A (Figure S6C). In conclusion, our data suggest a specific physical association between Tsp2A and aPKC or Rack1.

Next, we examined how *Tsp2A* knockdown affects the protein levels of Rack1 and aPKC by immunostaining with anti-aPKC (Dollar et al., 2005) and anti-Rack1 (Kadmas et al., 2007) antibodies. Strikingly, the expression of *Tsp2A* RNAi in ISCs/EBs dramatically increases aPKC staining at the cell surface (Figures 7E–7H and S6D–S6G; two different RNAi lines used). With confocal microscopy at high magnification, it is quite apparent that aPKC staining is usually concentrated in tiny punctae on the membrane of wild-type ISCs/EBs (Figures 7G and S6F), whereas the signals increase and extend along the cell border when *Tsp2A* RNAi is expressed in ISCs/EBs (Figures 7H and S6G; quantification in Figures 7N and S6P). The induction of membrane-localized aPKC staining also occurs when *Tsp2A* RNAi is expressed in EBs or ECs under the control of *SGT* or *Myo1A^{ts}* drivers (Figures 7I, 7J, S6H, and S6I), suggesting that Tsp2A regulates the protein levels of aPKC in different cell types in the ISC-EC lineage. Moreover, membrane-localized aPKC staining in ISCs/EBs increases significantly when the flies are fed with bleomycin food for 2 days (Figure 7O), which is consistent with the observation that most ISCs/EBs have not completed *de novo* Tsp2A-SJ assembly to become mature ECs at that time point following tissue damage (Figure S2O). The accumulation of aPKC on the cell membrane indicates a defect in endocytosis. Interestingly, a similar induction of membrane-localized aPKC is observed when endocytosis is nonspecifically inhibited with *Rab5* RNAi expression in ISCs/EBs (Figures S6J, S6K, S6J', and S6K'; quantification in Figure S6Q). In contrast, enhanced endocytosis by *Rab5^{ca}* expression can prevent the induction of membrane-localized aPKC staining following *Tsp2A* knockdown in ISCs/EBs (Figures 7K–7M and 7'–7M'; quantification in Figure 7P). Finally, in addition to aPKC, Rack1 staining signals also increase following *Tsp2A* knockdown or tissue damage (Figures S6L–S6O). Altogether, Tsp2A appears to facilitate the endocytic degradation and inactivation of aPKC or Rack1 during ISC-EC differentiation.

DISCUSSION

Characterization of Tsp2A in the adult *Drosophila* midgut reveals a pivotal link between EC maturation and the restriction of ISC proliferation (Figure S7). Progenitor cells differentiating toward ECs undergo a series of changes (Xu et al., 2018), which include the increase of nucleus ploidy and cell size, the formation of SJs, as well as the loss of concentrated aPKC staining at the cell surface. aPKC activity in ISCs/EBs, which increases following tissue damage, can help promote and sustain proliferation via Yki-JAK-Stat signaling. Tsp2A assembly at SJs and its subsequent internalization facilitate aPKC or Rack1 degradation and downregulate aPKC activity. Therefore, in the regeneration process following tissue damage, Tsp2A-SJ assembly not only allows EC maturation but also signals ISCs to reduce proliferation activity when enough mature ECs have been produced for tissue repair. Defects in *Tsp2A* expression cause excessive aPKC-Yki-JAK-Stat activity and make the midgut epithelia highly proliferative, like a wound that cannot heal.

Endocytic Regulation and Tetraspanin Family Proteins

Endocytosis controls the abundance of transmembrane or membrane-associated molecules. Whereas most internalized proteins and lipids are recycled and return to the cell surface, some are delivered to late endosomes and eventually degraded in lysosomes (Maxfield and McGraw, 2004). Disruption of endocytic degradation often results in excessive accumulation of signaling molecules and overproliferation. For example, the leucine-rich repeat (LRR) protein Windpipe promotes endocytic degradation of Dome, the receptor of mitogenic JAK-Stat pathway, in both the eye discs and the midgut epithelium (Ren et al., 2015). Our study elucidated the functional relevance for the endocytosis of the SJ protein Tsp2A and identified specific components (i.e., aPKC and Rack1) that connect Tsp2A to Hippo signaling, the core pathway restricting ISC activity in the midgut.

There are 38 and 33 tetraspanin proteins encoded by the *Drosophila* and mammalian genomes, respectively, many of which are known to regulate endocytic processes (Han et al., 2012; Pols and Klumperman, 2009; Xu et al., 2004). In addition to *Tsp2A*, our RNAi screen included lines targeting 16 more tetraspanins and identified *Tsp86D* to be required in ISCs/EBs for midgut proliferation and *Tsp42Ea* to be a weak ISC/EB tumor suppressor (data not shown). Moreover, our suppressor screen revealed that overexpression of *Tsp3A* can enhance *Tsp2A* RNAi-induced overproliferation, whereas *Tsp42Ef* inhibits *Tsp2A* RNAi-induced overproliferation (Table S2). Both Tsp86D and Tsp3A are known to affect Notch activation by regulating membrane trafficking of the metalloprotease ADAM10 or Kuzbanian to the cell surface (Dornier et al., 2012). Tsp42Ea is an ortholog of human CD63, with the potential to promote endocytic degradation (Pols and Klumperman, 2009). Moreover, Tsp42Ef, localized at multivesicular bodies (MVBs), might also participate in endocytic regulation (Gross et al., 2012). Given that different tetraspanins often interact with each other (Charrin et al., 2014), future studies of these additional tetraspanins (i.e., Tsp86D, Tsp42Ea, Tsp3A, and Tsp42Ef), including the development of reagents to visualize their endogenous expression in the midgut, might lead to a comprehensive understanding of Tsp2A trafficking to the SJs, Tsp2A internalization, and/or Tsp2A downstream signaling.

Different Junction Proteins Implicated in Epithelial Tissue Organization and Signaling

Cell junctions between polarized epithelial cells mediate paracellular permeability and cell attachment. In both *Drosophila* and mammals, AJs are located at the apical side of the lateral membrane and consist of a cadherin-catenin complex connected to the cytoskeleton (Sun and Irvine, 2016). In mammals, TJs are positioned apically to AJs and form the paracellular diffusion barrier (Zihni et al., 2016). Although insect cells do not have TJs, many TJ protein orthologs are found at SJs (Wei and Ellis, 2001; Wu et al., 2004). In the *Drosophila* midgut, AJs are enriched in ISCs/EBs (Choi et al., 2011), whereas SJs are predominantly distributed among ECs (Resnik-Docampo et al., 2017). A previous study identified *esg*-binding sites in the promoter of *Ssk* and found that *esg* suppresses the expression of multiple SJ-encoding genes (*Mesh*, *Ssk*, and *cora*) (Korzelius et al., 2014). Our detailed characterization of *Tsp2A* expression and function during ISC-EC differentiation confirms earlier speculation that upregulation of SJ components might be an important early step in EC differentiation (Korzelius et al., 2014). Interestingly, during the revision of our manuscript, SJ proteins were reported to be required for epithelial polarity in the midgut (Chen et al., 2018). Our

findings complement this study and provide further insight into the mechanisms of how the switch of cell polarity determinants from aPKC to SJs occurs during ISC-EC differentiation.

In addition to their structural roles in organizing the epithelium, junction proteins can participate in signal transduction. For example, *shotgun* knockdown in ISCs/EBs causes a mild increase in proliferation (Choi et al., 2011). *shotgun* knockdown in ECs induces *rhomboid* expression to facilitate secretion of mitogenic EGFs, causing feedback upregulation of EGFR-Ras-MAPK signaling and ISC proliferation (Liang et al., 2017). Moreover, a recent study found that disruption of SJs by *Gli* knockdown impairs intestinal barrier function in old flies and causes JNK-dependent induction of ISC proliferation (Resnik-Docampo et al., 2017). Unlike the work on *Gli*, we focused on the young adult stages and found that *Tsp2A* knockdown causes no defects in intestinal barrier function yet induces a strong overproliferation phenotype that cannot be rescued by JNK inhibition. In our study, we compared the knockdown effects of different junction proteins and demonstrated that the tumor suppressor role of SJ proteins is distinct from other types of junction proteins such as Arm, Lgl, and Gli.

In mammalian epithelial tissues such as the trachea, basal cells (stem cells) do not express the TJ proteins ZO1 and claudin-4 under normal conditions but can initiate TJ assembly when they are induced to differentiate after tissue damage (Gao et al., 2015). The kinetics of TJ protein expression in the process of tracheal progenitor cell differentiation is reminiscent of our observation with *Tsp2A* in the midgut. In the mammalian epithelium, the putative *Tsp2A* orthologs CD81, CD9, and CD151 localize to cell junctions (Lazo, 2007), whereas both CD81 and CD9 associate with claudins (Farquhar et al., 2012; Kovalenko et al., 2007). Moreover, CD81 and claudins can undergo internalization in mammalian epithelial cells (Farquhar et al., 2012; Matsuda et al., 2004). Given the similarity between *Tsp2A* and its mammalian orthologs, it will be interesting to examine whether the connection we have elucidated between SJ proteins and Hippo pathway could be generally applicable to TJ proteins in various mammalian epithelial tissues.

Tsp2A-aPKC-Hippo Signaling: Potential Implication in Cancer

Consistent with our discovery that *Tsp2A* suppresses epithelial cell proliferation, predicted *Tsp2A* orthologs such as CD81, CD9, and CD151 are often downregulated in carcinomas: *CD81* is frequently deleted in cancers (Broad Institute Tumorscape Project; Beroukhim et al., 2010), with its expression reduced in bladder, liver, and gastric carcinomas (Inoue et al., 2001; Lee et al., 2015; Yoo et al., 2013); *CD9* expression decreases in breast, ovarian, lung, esophageal, and colon carcinomas (Funakoshi et al., 2003; Houle et al., 2002; Miyake et al., 1996; Mori et al., 1998; Uchida et al., 1999); and *CD151* is downregulated in colon cancers (Chien et al., 2008). Moreover, both aPKC and Rack1 are known to play an oncogenic role in various carcinomas (Li and Xie, 2015; Mosesson et al., 2008). Whereas previous studies mostly focused on the function of *Tsp2A* orthologs in cell migration and cancer metastasis (Hemler, 2014), our findings suggest that *Tsp2A* orthologs might also be implicated in endocytic regulation to affect tumorigenesis.

Many small molecules can be ligands or antagonists for tetraspanins. For example, human CD81 has a binding pocket for cholesterol (Zimmerman et al., 2016), raising the possibility

that cholesterol could play a role in tumorigenesis by modulating the activity of CD81 or similar tetraspanins. Moreover, since CD81 is the receptor for hepatitis C virus (HCV) envelope protein and mediates HCV entry, there have been efforts to develop ligands or antibodies for CD81 or other putative Tsp2A orthologs (Rajesh et al., 2012). Based on our findings, products from these antiviral studies might be valuable for cancer research and treatment. Finally, our observation that tuning down aPKC or JAK-Stat activity can prevent ISCs expressing *Tsp2A* RNAi from overproliferating without blocking their normal regenerative response raises the possibility to treat cancer by converting hyperplastic ISCs into normal ISCs.

STAR★METHODS

KEY RESOURCES TABLE

REAGENT or RESOURCE	SOURCE	IDENTIFIER
Antibodies		
rabbit anti- β -galactosidase	Cappel	Cat#0855976
rabbit anti-pH3	Millipore	Cat#06-570; RRID:AB_310177
mouse anti-GFP	Invitrogen	Cat#A11120; RRID:AB_221568
rabbit anti-GFP	Invitrogen	Cat#A6455; RRID:AB_221570
mouse anti-Flag	Sigma	Cat#F3165; RRID:AB_259529
rabbit anti-cleaved-caspase 3	Cell Signaling	Cat#9661; RRID:AB_2341188
rabbit anti-Tsp2A	Izumi et al., 2016	N/A
rabbit anti-Mesh	Izumi et al., 2016	N/A
rabbit anti-Ssk	Izumi et al., 2016	N/A
rabbit anti-Cora	DSHB	Cat#C615.16; RRID:AB_1161644
mouse anti-Arm	DSHB	Cat#N27A1; RRID:AB_528089
rabbit anti-Lgl	Santa Cruz	Cat#sc-98260; RRID:AB_1564606
rabbit anti-Pdm1	Xiaohang Yang	N/A
mouse anti-Pros	DSHB	Cat#MR1A; RRID:AB_528440
mouse anti-Hrs	DSHB	Cat#27-4; RRID:AB_2618261
mouse anti-Rab7	DSHB	Cat#Rab7; RRID:AB_2722471
guinea pig anti-ex	Richard Fehon	Maitra et al., 2006
rabbit anti-aPKC	Santa Cruz	Cat#sc-216
rabbit anti-Rack1	Julie Kadrmas	Kadrmas et al., 2007
rat anti-HA (clone 3F10)	Sigma	Cat#11867423001; RRID:AB_390919
donkey anti-rabbit IgG, Alexa Fluor 488	Invitrogen	Cat#A21206; RRID:AB_141708
donkey anti-rabbit IgG, Alexa Fluor 594	Invitrogen	Cat#A21207; RRID:AB_141637
donkey anti-mouse IgG, Alexa Fluor 488	Invitrogen	Cat#A21202; RRID:AB_141607
donkey anti-mouse IgG, Alexa Fluor 594	Invitrogen	Cat#A21203; RRID:AB_141633
donkey anti-guinea pig IgG, Alexa Fluor 594	Jackson ImmunoResearch Labs	RRID:AB_2340474
goat anti-rat IgG, Alexa Fluor 488	Invitrogen	Cat#A11006; RRID:AB_141373
rabbit anti-GFP	Abcam	Cat#6556; RRID:AB_305564
rabbit anti-GFP	Invitrogen	Cat#A6455

REAGENT or RESOURCE	SOURCE	IDENTIFIER
GFP-Trap agarose beads	Bulldog Biotechnology	Cat#GTA100
Chemicals, Peptides, and Recombinant Proteins		
Paraformaldehyde 16% solution	Electron Microscopy Sciences	Cat#15710
PBS pH 7.4	GIBCO	Cat#10010023
Bleomycin	Calbiochem	Cat#203408
blue dye no.1	Spectrum Chemical	Cat#3844-45-9
Texas Red-avidin	Invitrogen	Cat#A820
Lysotracker Red DND-99	Invitrogen	Cat#L-7528
TRIzol Reagent	Invitrogen	Cat#15596018
RNase-Free DNase I Set	QIAGEN	Cat#79254
iScript Reverse Transcription Supermix	Bio-Rad	Cat#1708896
iQ SYBR Green Supermix	Bio-Rad	Cat#1708880
Cyclohexamide	Sigma	Cat#C7698
RNaseOUT ribonuclease inhibitor	Invitrogen	Cat#10777019
cOmplete Protease Inhibitor, EDTA-free	Roche	Cat#11836170001
Gateway LR Clonase II Enzyme mix	Invitrogen	Cat#11791-020
pENTR/D-TOPO Cloning Kit	Invitrogen	Cat#K2400-20
Effectene Transfection Reagent	QIAGEN	Cat#301425
GIBCO Schneider's <i>Drosophila</i> Sterile Medium	Thermo Fisher	Cat#21720024
Fetal Bovine Serum	Thermo Fisher	Cat#10437028
Protease and phosphatase inhibitor cocktail	Pierce	Cat#78440
Critical Commercial Assays		
RNeasy Mini kit	QIAGEN	Cat#74104
RNeasy MinElute Cleanup kit	QIAGEN	Cat#74204
4%–20% Mini-PROTEAN TGX Precast Protein Gels	Bio-Rad	Cat#4561096
Experimentl Models: Cell Lines		
<i>D. melanogaster</i> : Cell line S2R+	Perrimon lab	N/A
Experimental Models: Organisms/Strains		
<i>D. melanogaster</i> : UAS-Tsp2A sgRNA	This paper	N/A
<i>D. melanogaster</i> : UAS-FH-Tsp2A	This paper	N/A
<i>D. melanogaster</i> : UAS-GFP-Tsp2A	This paper	N/A
<i>D. melanogaster</i> : DI-lacZ	BDSC	11651
<i>D. melanogaster</i> : y v; attP2 (Ctrl ^{bl})	BDSC	36303
<i>D. melanogaster</i> : UAS-Luc RNAi	BDSC	31603
<i>D. melanogaster</i> : UAS-Tsp2A RNAi	BDSC	40899
<i>D. melanogaster</i> : UAS-Luc	BDSC	35789
<i>D. melanogaster</i> : FRT19A	BDSC	1744
<i>D. melanogaster</i> : UAS-bsk RNAi	BDSC	31323, 32977 (#2)
<i>D. melanogaster</i> : UAS-bsk ^{DN}	BDSC	6409
<i>D. melanogaster</i> : UAS-GFP-RpL10Ab	BDSC	42683

REAGENT or RESOURCE	SOURCE	IDENTIFIER
<i>D. melanogaster</i> : UAS-rpr	BDSC	5823
<i>D. melanogaster</i> : UAS-Hep ^{ca}	BDSC	6406
<i>D. melanogaster</i> : UAS-CD8-GFP	BDSC	32186
<i>D. melanogaster</i> : UAS-Rab5 ^{ca}	BDSC	43335
<i>D. melanogaster</i> : UAS-YFP-Rab5 ^{ca}	BDSC	9773
<i>D. melanogaster</i> : UAS-Rab7 ^{ca}	BDSC	42707
<i>D. melanogaster</i> : UAS-YFP-Rab11 ^{ca}	BDSC	50783
<i>D. melanogaster</i> : UAS-Rab5 ^{DN}	BDSC	42704
<i>D. melanogaster</i> : UAS-YFP-Rab7 ^{DN}	BDSC	9778
<i>D. melanogaster</i> : UAS-YFP-Rab11 ^{DN}	BDSC	23261
<i>D. melanogaster</i> : UAS-Rab5 RNAi	BDSC	30518
<i>D. melanogaster</i> : UAS-Rab7 RNAi	BDSC	27051
<i>D. melanogaster</i> : UAS-Rab11 RNAi	BDSC	42709, 27730 (#2)
<i>D. melanogaster</i> : UAS-arm RNAi	BDSC	31305, 31304 (#2)
<i>D. melanogaster</i> : UAS-Lgl RNAi	BDSC	35773, 38989 (#2)
<i>D. melanogaster</i> : UAS-cora RNAi	BDSC	28933, 51845 (#2)
<i>D. melanogaster</i> : UAS-Gli RNAi	BDSC	38284, 58115 (#2)
<i>D. melanogaster</i> : UAS-aPKC RNAi	BDSC	34332, 35001 (#2)
<i>D. melanogaster</i> : UAS-Rack1 RNAi	BDSC	34694
<i>D. melanogaster</i> : UAS-aPKC ^{DN}	BDSC	51673
<i>D. melanogaster</i> : UAS-Yki ^{3SA}	BDSC	28817
<i>D. melanogaster</i> : UAS-Yki RNAi	BDSC	31965
<i>D. melanogaster</i> : UAS-hpo	BDSC	44254
<i>D. melanogaster</i> : UAS-dome RNAi	BDSC	32860
<i>D. melanogaster</i> : UAS-Stat92E RNAi	BDSC	33637
<i>D. melanogaster</i> : hop ²	BDSC	6032
<i>D. melanogaster</i> : hop ²⁷	BDSC	8493
<i>D. melanogaster</i> : y w; attP (Ctrl ^y)	VDRC	60100
<i>D. melanogaster</i> : UAS-Mesh RNAi ^v	VDRC	108297
<i>D. melanogaster</i> : UAS-Ssk RNAi ^v	VDRC	11906, 105193 (#2)
<i>D. melanogaster</i> : UAS-Yki RNAi ^v	VDRC	104523
<i>D. melanogaster</i> : UAS-Tsp2A RNAi ^N	NIG	11415R-2
<i>D. melanogaster</i> : UAS-Rack1-3xHA	FlyORF	F001043
<i>D. melanogaster</i> : UAS-aPKC-3xHA	FlyORF	F000876
<i>D. melanogaster</i> : y w (Ctrl ^{yw})	Perrimon lab	N/A
<i>D. melanogaster</i> : w1118 (Ctrl ^w)	Perrimon lab	N/A
<i>D. melanogaster</i> : Diap1-lacZ/TM6B	Karpowicz et al., 2010	N/A
<i>D. melanogaster</i> : UAS-p35 (on 3 rd chromosome)	Perrimon lab	N/A
<i>D. melanogaster</i> : esgGal4 UAS-GFP tubGal80 ^{ts} (EGT)	Micchelli and Perrimon, 2006	N/A
<i>D. melanogaster</i> : EGT; UAS-Cas9 (attP2)	Perrimon lab	N/A

REAGENT or RESOURCE	SOURCE	IDENTIFIER
<i>D. melanogaster</i> : esgGal4 tubGal80 ^{ts} (esg ^{ts})	Perrimon lab	N/A
<i>D. melanogaster</i> : Myo1AGal4 tubGal80 ^{ts} (Myo1A ^{ts})	Perrimon lab	N/A
<i>D. melanogaster</i> : tubGal80 ^{ts} ; 24BGal4 (24B ^{ts})	Perrimon lab	N/A
<i>D. melanogaster</i> : tubGal80 ^{ts} ; DaGal4 (Da ^{ts})	Perrimon lab	N/A
<i>D. melanogaster</i> : tubGal80 ^{ts} ; DIGal4 (DI ^{ts})	Zeng et al., 2010	N/A
<i>D. melanogaster</i> : tubGal80 ^{ts} ; Su(H)Gbe-Gal4 (Su(H) ^{ts})	Zeng et al., 2010	N/A
<i>D. melanogaster</i> : Su(H)Gbe-Gal4, UAS-CD8-GFP; tubGal80 ^{ts} (SGT)	Zeng et al., 2010	N/A
<i>D. melanogaster</i> : tubGal80 ^{ts} ; ProsGal4 (Pros ^{ts})	Perrimon lab	N/A
<i>D. melanogaster</i> : hsFlp tubGal80 FRT19A/FM7; tubGal4 UAS-mCD8::GFP/TM3	Choi et al., 2011	N/A
Oligonucleotides		
<i>Tsp2A</i> sgRNAs	This paper	See Table S3
RT-qPCR primers	This paper	See Table S3
Recombinant DNA		
cDNA RE51204	Drosophila Genomics Resource Center	9398
cDNA FI03288	Drosophila Genomics Resource Center	1621950
cDNA RE74715	Drosophila Genomics Resource Center	10113
pENTR/D-TOPO-Tsp2A	This paper	N/A
pENTR/D-TOPO-aPKC	This paper	N/A
pENTR/D-TOPO-Rack1	This paper	N/A
pAGW-Tsp2A	This paper	N/A
pAFW-Tsp2A	This paper	N/A
pAGW-aPKC	This paper	N/A
pAFW-aPKC	This paper	N/A
pAGW-Rack1	This paper	N/A
pAFW-Rack1	This paper	N/A
Software and Algorithms		
ZEN 2 lite	Zeiss	N/A
ImageJ/Fiji	Schindelin et al., 2012	N/A
CFX Manager	Bio-Rad	N/A
STREAM	Chen et al., 2018	N/A
Prism	GraphPad Software	N/A
Other		
Zeiss LSM780 microscope	Zeiss	N/A
CFX96 Real-Time System	Bio-Rad	N/A
BZ-9000 Fluorescence Microscope	Keyence	N/A

REAGENT or RESOURCE	SOURCE	IDENTIFIER
1200-EX transmission electron microscope	JEOL	N/A

CONTACT FOR REAGENT AND RESOURCE SHARING

Further information and requests for resources and reagents should be directed to and will be fulfilled by the Lead Contact, Norbert Perrimon (perrimon@receptor.med.harvard.edu).

EXPERIMENTAL MODEL AND SUBJECT DETAILS

***Drosophila* culture**—Flies were reared on standard cornmeal/agar medium. Fly food was changed every two days to keep fresh. Conditional expression in adult flies using *tubGal80^{ts}* was achieved by maintaining flies at 18°C until 4–7 days after eclosion, and then shifting young adults to 29°C. For MARCM experiments, flies were reared at 18°C until 3–5 days after eclosion, heat-shocked at 37°C for 1 hr, and then maintained back at 18°C for 10d before dissection and analysis. For consistency, female adult flies, whose midguts are larger and easier to dissect, were analyzed in this paper. To induce tissue damage, fly cornmeal/agar food was melted and mixed well with a final concentration of 25 µg/ml bleomycin.

Transgenic flies—The cDNA of *Tsp2A* was cloned into pTFHW or pTGW expression vectors (the *Drosophila* Gateway Vector collection) to generate *UAS-FH-Tsp2A* and *UAS-GFP-Tsp2A* transgenic flies.

A pair of sgRNAs targeting the coding region of *Tsp2A* were designed and cloned into the double U6-sgRNA vector pCFD4 (Port et al., 2014) for site-specific insertion into attP2 on the 3rd chromosome. We obtained transgenic flies ubiquitously expressing two sgRNAs with the seed sequences listed in Table S3.

METHOD DETAILS

Staining and fluorescence imaging—For immunostainings, *Drosophila* midguts were dissected in PBS, fixed in 4% paraformaldehyde in PBS for 1 hr, incubated for 1–2 hr in Blocking Buffer [5% Normal Donkey Serum (with additional 5% Normal Goat Serum when goat-anti-rat secondary antibody was used), 0.3% Triton X-100, 0.1% BSA in PBS], and stained overnight at 4°C in PBST [0.3% Triton X-100, 0.1% BSA in PBS] with any of the following primary antibodies:

Rabbit anti-β-galactosidase (1:6000), rabbit anti-pH3 (1:3000), mouse anti-GFP (1:300), rabbit anti-GFP (Invitrogen; 1:500), mouse anti-Flag (1:1000), rabbit anti-cleaved-caspase 3 (1:500), rabbit anti-Tsp2A (1:2000), rabbit anti-Mesh (1:1000), rabbit anti-Ssk (1:1000), rabbit anti-Cora (1:50), mouse anti-Arm (1:20), rabbit anti-Lgl (1:300), rabbit anti-Pdm1 (1:500), mouse anti-Pros (1:50), mouse anti-Hrs (1:40), mouse anti-Rab7 (1:40), guinea pig anti-ex (1:2000), rabbit anti-aPKC (1:100), rabbit anti-Rack1 (1:500), rat anti-HA (1:1000).

After primary antibody staining, the midguts were washed 3 times with PBST, stained with DAPI (1:2000) and Alexa Fluor- conjugated donkey-anti-mouse, donkey-anti-rabbit, goat-

anti-rat, or donkey-anti-guinea pig secondary antibodies (1:1000) in PBST at 22°C for 2 hr, washed 3 times with PBST, and mounted in Vectashield medium on microscopic slides.

For mitosis quantification, the number of pH3+ cells in the entire midgut was counted with a regular epi-fluorescence microscope. The images of the entire midgut were captured with a Keyence microscope.

The endocytosis assay was adapted from the existing protocol (Shravage et al., 2013). Dissected midguts were incubated *ex vivo* with Texas Red-avidin diluted in adult hemolymph-like buffer [2 mM CaCl₂, 5 mM KCl, 5 mM HEPES, 8.2 mM MgCl₂, 108 mM NaCl, 4 mM NaHCO₃, 1 mM NaH₂PO₄, 10 mM Sucrose, 5 mM Trehalose, adjusted with NaOH to pH = 7.5] to a concentration of 80 µg/ml for 20 min, rinsed with PBS, fixed in 4% paraformaldehyde, and stained following a standard protocol.

Lysotracker staining was performed as previously described (Ren et al., 2009), midguts were dissected in PBS, incubated in 0.5 µM LysoTracker Red DND-99 for 3 min, rinsed, and then transferred to PBS on microscopic slides, and photographed immediately.

Images of the posterior midgut area were captured with a Zeiss LSM780 confocal microscope. A z stack of 10–20 images covering one layer of the epithelium from the apical to the basal side were acquired, adjusted, and assembled using NIH Fiji (ImageJ) (Schindelin et al., 2012), and shown as a maximum projection unless indicated otherwise.

For quantification of intracellular Tsp2A stainings, we encircled the intracellular region of an individual cell in the maximum projection image (excluding the surface stack) and measured with Fiji; For quantification of membrane-localized Tsp2A stainings in each cell, we took the sum of Tsp2A staining intensity at the cell surface Z stack and Tsp2A staining intensity at the cell border of the maximum projection image; For quantification of membrane-localized aPKC in each ISC/EB, we encircled the aPKC punctae or elongated aPKC staining along the cell border, and measured the total intensity using Fiji.

RT-qPCR—Total RNA was extracted from 15–20 midguts using TRIzol reagent, treated with DNase I, purified using the QIAGEN RNeasy Mini kit, and converted to cDNA using the iScript Reverse Transcription Supermix. The cDNA was analyzed by real-time quantitative PCR using the iQ SYBR Green Supermix. The sequences of RT-qPCR primers were listed in Table S3. *GAPDH* and *rp49* were used as the internal controls. Each RT-qPCR was performed with three technical replicates, and at least two biological replicates. Representative data (analyzed by Bio-Rad CFX Manager) are presented as mean ± SEM. For qPCR experiments, single asterisk (*) indicates significant difference ($p < 0.05$) between different groups of technical replicates.

Translating Ribosome Affinity Purification (TRAP) for RT-qPCR analysis—For TRAP experiments, *GFP-RpL10A* expression was induced in ISCs/EBs with *esg^{ΔS}* or in ECs with *Myo1A^{ΔS}* for 4d before dissection. $N > 400$ or $N > 30$ midguts were dissected in PBS for ISC/EB-specific or EC-specific TRAP, respectively. We used plastic Kimble Kontes pellet pestles to homogenize dissected midguts in 500 mL Extraction Buffer [20 mM HEPES (pH7.5), 150 mM KCl, 5 mM MgCl₂, 1% Triton X-100, 0.5 mM DTT, 100 µg/ml

Cyclohexamide, 100 U/ml RNaseOUT, 1× cOmplete Protease Inhibitor] on ice. To get rid of the debris, lysates were centrifuged at 4°C twice, first for 5 min at 2000 rpm, then for 10 min at maximum speed. Supernatants were incubated for 2 hr at 4°C on a rotator with 50 µL GFP-Trap agarose beads (Bulldog Bio) that have been pre-equilibrated in Extraction Buffer for at least 30 min. Next, the beads were centrifuged at 4°C at 2000 rpm for 2 min, and washed 3 times (for 10 min each time) in Wash Buffer [150 mM NaCl, 0.05% Triton X-100, 50 mM Tris, 5 mM MgCl₂, 40 U/ml RNase OUT, 1× cOmplete Protease Inhibitor] at 4°C. After washing, the precipitated GFP-Trap beads were mixed and incubated with 100 µL TRIzol for 10 min, mixed thoroughly with 40 µL chloroform by repeated inverting, and centrifuged at 4°C at maximum speed for 10 min. The aqueous phase was used for RNA extraction using the QIAGEN RNeasy MinElute Cleanup kit (with on-column DNase I digestion). The RNA was converted to cDNA and used for qRT-PCR analysis. For TRAP RT-qPCR, *α-tubulin* was used as the internal control.

Smurf assay—Smurf assays were performed as previously described (Rera et al., 2012). Standard fly medium was mixed with blue dye no.1 at a concentration of 2.5% (wt/vol). Flies were maintained on dyed medium for 9 hr each time before analysis. A fly was counted as “Smurf positive” when blue dye could be observed outside of the digestive tract. Flies fed with food containing 1% SDS (Liang et al., 2017) for at least 3 days prior to the assay were used as positive controls.

Electron microscopy (EM) and EM with immunogold labeling—For regular EM, tissues of the posterior midgut were fixed in the fixative solution [2.5% Glutaraldehyde 1.25% Paraformaldehyde and 0.03% picric acid in 0.1 M sodium cacodylate buffer (pH 7.4)] for at least 2 hours at room temperature, washed in 0.1M cacodylate buffer and postfixed with 1% Osmiumtetroxide (OsO₄)/1.5% Potassiumferrocyanide (K₄Fe(CN)₆) for 1 hour, washed 2× in water, 1× Maleate buffer (MB) 1x and incubated in 1% uranyl acetate in MB for 1hr followed by 2 washes in water and subsequent dehydration in grades of alcohol (10min each; 50%, 70%, 90%, 2×10min 100%). The samples were then put in propyleneoxide for 30 minutes and infiltrated ON in a 1:1 mixture of propyleneoxide and TAAB Epon (Marivac Canada Inc. St. Laurent, Canada). The following day the samples were embedded in TAAB Epon and polymerized at 60°C for 48 hr. Ultrathin plastic sections (~60nm) were cut on a Reichert Ultracut-S microtome, picked up on to copper grids, and contrasted with 0.3% lead citrate. Grids with the plastic sections were imaged using a JEOL 1200-EX transmission electron microscope operating at 80 kV with an AMT 2k CCD camera. Representative images from more than 3 different midgut sections are presented in figures.

For EM with immunogold labeling, tissues of the posterior midgut were fixed for 2 hr in 0.1 M sodium phosphate buffer (pH = 7.4) containing fresh 4% paraformaldehyde and 0.2% glutaraldehyde, rinsed in PBS, and then either processed with 2.3 M sucrose cryo-protection and frozen in liquid nitrogen, or processed with osmium fixation and plastic embedding. Frozen or plastic-embedded samples were cut into ~80 nm sections using a Reichert Ultracut S microtome and transferred to formvar-carbon coated copper grids. Unless specified otherwise, staining was performed at 22°C. Frozen sections were blocked in 1% BSA/PBS

buffer for 10 min, incubated with anti-GFP antibody (1:30, Abcam 6556) in 1% BSA/PBS for 1 h, washed 4 times in PBS, incubated with protein A-conjugated 15 nm gold particles for 20 min, washed 2 times in PBS and 4 times in water, and incubated in a mixture of 0.3% uranyl acetate and 2% methyl cellulose for 5 min for contrasting/ embedding. Plastic sections were etched in saturated sodium m-periodate (SIGMA) for 3 min, washed 3 times in water, blocked in PBT buffer [0.1% Triton X-100, 1% BSA in PBS] for 30 min, incubated with anti-GFP antibody (Abcam; 1:50) in PBT at 4°C overnight, washed 4 times in PBS, incubated with protein A-conjugated 15 nm gold particles for 20 min, washed 2 times in PBS and 4 times in water, and stained with lead citrate. Grids with frozen or plastic sections were imaged the same way as regular EM.

Single-cell RNA-seq and data processing—Details on the adult midgut single-cell RNA-seq are described in (Hung et al., 2018). In brief, 1753 midgut cells with good sequencing quality were clustered the cells via Seurat analysis (Butler et al., 2018) into separate groups corresponding to 443 ISC/EBs, 196 EEs, 1053 ECs, and 61 other non-epithelial cells. Single-cell trajectory reconstruction was performed using STREAM (<http://stream.pinellolab.org/>), with the S2 state expressing high levels of ISC markers selected as the starting state. Trajectories were displayed as a 3D scattered plot and projected in 2D. The genes of interests are visualized as individual 2D STREAM plots.

Co-immunoprecipitation—cDNAs of *Tsp2A* (RE51204), *aPKC* (FI03288, isoform RA) and *Rack1* (RE74715, isoform RA) were cloned into actin promoter-driven pAGW and pAFW expression vectors obtained from the *Drosophila* Gateway Vector collection. S2R+ cells were cultured in Schneider's medium supplemented with 10% fetal bovine serum (FBS) at 25°C. DNA was transfected into S2R+ cells in a 10 cm plate using Effectene transfection reagent. After 3 d of incubation, cells were lysed with Lysis Buffer [30 mM pH = 7.5 Tris-HCl, 150 mM NaCl, 1% Brij97 (P6136, Sigma-Aldrich, St. Louis, MO, USA)] with halt protease and phosphatase inhibitor cocktail (Pierce). Lysates were incubated with GFP-Trap beads for 1–2 hr at 4°C to precipitate the protein complexes. Beads were washed 3 times with 1 mL lysis buffer. Protein complexes were detected by western blotting using rabbit anti-GFP (Invitrogen; 1:5000) and mouse anti-Flag (1:5000).

QUANTIFICATION AND STATISTICAL ANALYSIS

For statistical analyses in all but qPCR experiments, the average value and the standard error of the mean (SEM) of biological replicates were calculated with Microsoft Excel and shown in the figures. For comparison of any two data groups, p values were calculated by Student's two-tail t test with unequal variances. Single asterisk (*) indicates a p value that is more than 0.01 but less than 0.05. Double asterisks (**) label a p value that is more than 0.001 but less than 0.01. Triple asterisks (***) label a p value that is less than 0.001. The p value of more than 0.1 is labeled as “not significant” (n.s.). For experiments with multiple data groups, one-way ANOVA with Bonferroni's multiple comparisons test (using GraphPad Prism) was performed to confirm the significant differences (of less or equal p value) as labeled in Figures. No particular methods were used to determine whether the data met assumptions of the statistical approach. Sample sizes, determined empirically and by convenience, are

documented in the figure legends. The raw data used for quantification in each Figure are documented in Table S4.

Supplementary Material

Refer to Web version on PubMed Central for supplementary material.

ACKNOWLEDGMENTS

We thank Allison Bardin, Steve Hou, and Ben Ohlstein for sharing fly stocks and Yasushi Izumi, Richard Fehon, Kim McCall, and Julie Kadrmas for antibodies. We thank Martin Hemler and Fernando Camargo for discussions, the Microscopy Resources on the North Quad (MicRoN) core at Harvard Medical School for confocal imaging support, and Maria Ericsson and the Harvard Medical School EM Facility for electron microscopy support. We also thank Perrimon lab members, especially Young Kwon, Phillip Karpowicz, Mary-Lee Deque´ant, and Richelle Sopko, for discussion and technical instructions; Christians Villalta for transgenic fly injections; and Stephanie Mohr, Afroditi Petsakou, Richard Binari, David Doupe´, and Li He for comments on the manuscript. Work in the Perrimon lab is supported by NIGMS (grant GM067761), the STARR consortium, and HHMI. N.P. is an Investigator of the Howard Hughes Medical Institute. H.-W.T. is supported by the Human Frontier Science Program. R.-J.H. is supported by the Jane Coffin Childs Foundation.

REFERENCES

- Amcheslavsky A, Jiang J, and Ip YT (2009). Tissue damage-induced intestinal stem cell division in *Drosophila*. *Cell Stem Cell* 4, 49–61. [PubMed: 19128792]
- Archibald A, Al-Masri M, Liew-Spilger A, and McCaffrey L (2015). Atypical protein kinase C induces cell transformation by disrupting Hippo/Yap signaling. *Mol. Biol. Cell* 26, 3578–3595. [PubMed: 26269582]
- Beroukhi R, Mermel CH, Porter D, Wei G, Raychaudhuri S, Donovan J, Barretina J, Boehm JS, Dobson J, Urashima M, et al. (2010). The land scape of somatic copy-number alteration across human cancers. *Nature* 463, 899–905. [PubMed: 20164920]
- Betschinger J, Mechtler K, and Knoblich JA (2003). The Par complex directs asymmetric cell division by phosphorylating the cytoskeletal protein Lgl. *Nature* 422, 326–330. [PubMed: 12629552]
- Bilder D, and Perrimon N (2000). Localization of apical epithelial determinants by the basolateral PDZ protein Scribble. *Nature* 403, 676–680. [PubMed: 10688207]
- Bilder D, Li M, and Perrimon N (2000). Cooperative regulation of cell polarity and growth by *Drosophila* tumor suppressors. *Science* 289, 113–116. [PubMed: 10884224]
- Butler A, Hoffman P, Smibert P, Papalexi E, and Satija R (2018). Integrating single-cell transcriptomic data across different conditions, technologies, and species. *Nat. Biotechnol* 36, 411–420. [PubMed: 29608179]
- Cai J, Zhang N, Zheng Y, de Wilde RF, Maitra A, and Pan D (2010). The Hippo signaling pathway restricts the oncogenic potential of an intestinal regeneration program. *Genes Dev* 24, 2383–2388. [PubMed: 21041407]
- Charrin S, Jouannet S, Boucheix C, and Rubinstein E (2014). Tetraspanins at a glance. *J. Cell Sci* 127, 3641–3648. [PubMed: 25128561]
- Chen H, Albergante L, Hsu JY, Lareau CA, Bosco GL, Guan J, Zhou S, Gorban AN, Bauer DE, Aryee MJ, et al. (2018). STREAM: single-cell trajectories reconstruction, exploration and mapping of omics data. *bioRxiv* 10.1101/302554.
- Chen J, Sayadian AC, Lowe N, Lovegrove HE, and St Johnston D (2018). An alternative mode of epithelial polarity in the *Drosophila* midgut. *PLoS Biol* 16, e3000041. [PubMed: 30339698]
- Chien CW, Lin SC, Lai YY, Lin BW, Lin SC, Lee JC, and Tsai SJ (2008). Regulation of CD151 by hypoxia controls cell adhesion and metastasis in colorectal cancer. *Clin. Cancer Res* 14, 8043–8051. [PubMed: 19073968]
- Choi NH, Lucchetta E, and Ohlstein B (2011). Nonautonomous regulation of *Drosophila* midgut stem cell proliferation by the insulin-signaling pathway. *Proc. Natl. Acad. Sci. USA* 108, 18702–18707. [PubMed: 22049341]

- Deng Y, Matsui Y, Zhang Y, and Lai ZC (2013). Hippo activation through homodimerization and membrane association for growth inhibition and organ size control. *Dev. Biol* 375, 152–159. [PubMed: 23298890]
- Dollar GL, Weber U, Mlodzik M, and Sokol SY (2005). Regulation of Lethal giant larvae by Dishevelled. *Nature* 437, 1376–1380. [PubMed: 16251968]
- Dornier E, Coumailleau F, Ottavi JF, Moretti J, Boucheix C, Mauduit P, Schweisguth F, and Rubinstein E (2012). TspanC8 tetraspanins regulate ADAM10/Kuzbanian trafficking and promote Notch activation in flies and mammals. *J. Cell Biol* 199, 481–496. [PubMed: 23091066]
- Doupe DP, Marshall OJ, Dayton H, Brand AH, and Perrimon N (2018). Drosophila intestinal stem and progenitor cells are major sources and regulators of homeostatic niche signals. *Proc. Natl. Acad. Sci. USA* 115, 12218–12223. [PubMed: 30404917]
- Farquhar MJ, Hu K, Harris HJ, Davis C, Brimacombe CL, Fletcher SJ, Baumert TF, Rappoport JZ, Balfe P, and McKeating JA (2012). Hepatitis C virus induces CD81 and claudin-1 endocytosis. *J. Virol* 86, 4305–4316. [PubMed: 22318146]
- Funakoshi T, Tachibana I, Hoshida Y, Kimura H, Takeda Y, Kijima T, Nishino K, Goto H, Yoneda T, Kumagai T, et al. (2003). Expression of tetraspanins in human lung cancer cells: frequent downregulation of CD9 and its contribution to cell motility in small cell lung cancer. *Oncogene* 22, 674–687. [PubMed: 12569360]
- Gao X, Bali AS, Randell SH, and Hogan BL (2015). GRHL2 coordinates regeneration of a polarized mucociliary epithelium from basal stem cells. *J. Cell Biol* 211, 669–682. [PubMed: 26527742]
- Green KJ, Getsios S, Troyanovsky S, and Godsel LM (2010). Intercellular junction assembly, dynamics, and homeostasis. *Cold Spring Harb. Perspect. Biol* 2, a000125. [PubMed: 20182611]
- Gregorieff A, Liu Y, Inanlou MR, Khomchuk Y, and Wrana JL (2015). Yap-dependent reprogramming of Lgr5(+) stem cells drives intestinal regeneration and cancer. *Nature* 526, 715–718. [PubMed: 26503053]
- Grivennikov S, Karin E, Terzic J, Mucida D, Yu GY, Vallabhapurapu S, Scheller J, Rose-John S, Cheroutre H, Eckmann L, and Karin M (2009). IL-6 and Stat3 are required for survival of intestinal epithelial cells and development of colitis-associated cancer. *Cancer Cell* 15, 103–113. [PubMed: 19185845]
- Gross JC, Chaudhary V, Bartscherer K, and Boutros M (2012). Active Wnt proteins are secreted on exosomes. *Nat. Cell Biol* 14, 1036–1045. [PubMed: 22983114]
- Grzeschik NA, Parsons LM, Allott ML, Harvey KF, and Richardson HE (2010). Lgl, aPKC, and Crumbs regulate the Salvador/Warts/Hippo pathway through two distinct mechanisms. *Curr. Biol* 20, 573–581. [PubMed: 20362447]
- Han SY, Lee M, Hong YK, Hwang S, Choi G, Suh YS, Park SH, Lee S, Lee SH, Chung J, et al. (2012). Tsp66E, the Drosophila KAI1 homologue, and Tsp74F function to regulate ovarian follicle cell and wing development by stabilizing integrin localization. *FEBS Lett* 586, 4031–4037. [PubMed: 23068610]
- He L, Si G, Huang J, Samuel ADT, and Perrimon N (2018). Mechanical regulation of stem-cell differentiation by the stretch-activated Piezo channel. *Nature* 555, 103–106. [PubMed: 29414942]
- Hemler ME (2005). Tetraspanin functions and associated microdomains. *Nat. Rev. Mol. Cell Biol* 6, 801–811. [PubMed: 16314869]
- Hemler ME (2014). Tetraspanin proteins promote multiple cancer stages. *Nat. Rev. Cancer* 14, 49–60. [PubMed: 24505619]
- Hong W, and Guan KL (2012). The YAP and TAZ transcription co-activators: key downstream effectors of the mammalian Hippo pathway. *Semin. Cell Dev. Biol* 23, 785–793. [PubMed: 22659496]
- Houle CD, Ding XY, Foley JF, Afshari CA, Barrett JC, and Davis BJ (2002). Loss of expression and altered localization of KAI1 and CD9 protein are associated with epithelial ovarian cancer progression. *Gynecol. Oncol* 86, 69–78. [PubMed: 12079303]
- Huang J, Wu S, Barrera J, Matthews K, and Pan D (2005). The Hippo signaling pathway coordinately regulates cell proliferation and apoptosis by inactivating Yorkie, the Drosophila homolog of YAP. *Cell* 122, 421–434. [PubMed: 16096061]

- Hung R, Hu Y, Kirchner R, Li F, Xu C, Comjean A, Tattikota S, Song W, Sui S, and Perrimon N (2018). A cell atlas of the adult *Drosophila* midgut. *bioRxiv* 10.1101/410423.
- Inoue G, Horiike N, and Onji M (2001). The CD81 expression in liver in hepatocellular carcinoma. *Int. J. Mol. Med* 7, 67–71. [PubMed: 11115611]
- Izumi Y, Motoishi M, Furuse K, and Furuse M (2016). A tetraspanin regulates septate junction formation in *Drosophila* midgut. *J. Cell Sci* 129, 1155–1164. [PubMed: 26848177]
- Jiang H, and Edgar BA (2011). Intestinal stem cells in the adult *Drosophila* midgut. *Exp. Cell Res* 317, 2780–2788. [PubMed: 21856297]
- Jiang H, Patel PH, Kohlmaier A, Grenley MO, McEwen DG, and Edgar BA (2009). Cytokine/Jak/Stat signaling mediates regeneration and homeostasis in the *Drosophila* midgut. *Cell* 137, 1343–1355. [PubMed: 19563763]
- Jiang H, Grenley MO, Bravo M-J, Blumhagen RZ, and Edgar BA (2011). EGFR/Ras/MAPK signaling mediates adult midgut epithelial homeostasis and regeneration in *Drosophila*. *Cell Stem Cell* 8, 84–95. [PubMed: 21167805]
- Kadmas JL, Smith MA, Pronovost SM, and Beckerle MC (2007). Characterization of RACK1 function in *Drosophila* development. *Dev. Dyn* 236, 2207–2215. [PubMed: 17584887]
- Karpowicz P, Perez J, and Perrimon N (2010). The Hippo tumor suppressor pathway regulates intestinal stem cell regeneration. *Development* 137, 4135–4145. [PubMed: 21098564]
- Korzelius J, Naumann SK, Loza-Coll MA, Chan JS, Dutta D, Oberheim J, Gläßer C, Southall TD, Brand AH, Jones DL, and Edgar BA (2014). Escargot maintains stemness and suppresses differentiation in *Drosophila* intestinal stem cells. *EMBO J* 33, 2967–2982. [PubMed: 25298397]
- Kovalenko OV, Yang XH, and Hemler ME (2007). A novel cysteine crosslinking method reveals a direct association between claudin-1 and tetraspanin CD9. *Mol. Cell. Proteomics* 6, 1855–1867. [PubMed: 17644758]
- Kwon Y, Song W, Droujinine IA, Hu Y, Asara JM, and Perrimon N (2015). Systemic organ wasting induced by localized expression of the secreted insulin/IGF antagonist ImpL2. *Dev. Cell* 33, 36–46. [PubMed: 25850671]
- Lazo PA (2007). Functional implications of tetraspanin proteins in cancer biology. *Cancer Sci* 98, 1666–1677. [PubMed: 17727684]
- Lee MS, Kim JH, Lee JS, Yun SJ, Kim WJ, Ahn H, and Park J (2015). Prognostic significance of CREB-binding protein and CD81 expression in primary high grade non-muscle invasive bladder cancer: identification of novel biomarkers for bladder cancer using antibody microarray. *PLoS ONE* 10, e0125405. [PubMed: 25915404]
- Li JJ, and Xie D (2015). RACK1, a versatile hub in cancer. *Oncogene* 34, 1890–1898. [PubMed: 24882575]
- Liang J, Balachandra S, Ngo S, and O'Brien LE (2017). Feedback regulation of steady-state epithelial turnover and organ size. *Nature* 548, 588–591. [PubMed: 28847000]
- Lin G, Zhang X, Ren J, Pang Z, Wang C, Xu N, and Xi R (2013). Integrin signaling is required for maintenance and proliferation of intestinal stem cells in *Drosophila*. *Dev. Biol* 377, 177–187. [PubMed: 23410794]
- Maitra S, Kulikauskas RM, Gavilan H, and Fehon RG (2006). The tumor suppressors Merlin and Expanded function cooperatively to modulate receptor endocytosis and signaling. *Curr. Biol* 16, 702–709. [PubMed: 16581517]
- Matsuda M, Kubo A, Furuse M, and Tsukita S (2004). A peculiar internalization of claudins, tight junction-specific adhesion molecules, during the intercellular movement of epithelial cells. *J. Cell Sci* 117, 1247–1257. [PubMed: 14996944]
- Maxfield FR, and McGraw TE (2004). Endocytic recycling. *Nat. Rev. Mol. Cell Biol* 5, 121–132. [PubMed: 15040445]
- Micchelli CA, and Perrimon N (2006). Evidence that stem cells reside in the adult *Drosophila* midgut epithelium. *Nature* 439, 475–479. [PubMed: 16340959]
- Miyake M, Nakano K, Itoi SI, Koh T, and Taki T (1996). Motility-related protein-1 (MRP-1/CD9) reduction as a factor of poor prognosis in breast cancer. *Cancer Res* 56, 1244–1249. [PubMed: 8640807]

- Mori M, Mimori K, Shiraishi T, Haraguchi M, Ueo H, Barnard GF, and Akiyoshi T (1998). Motility related protein 1 (MRP1/CD9) expression in colon cancer. *Clin. Cancer Res* 4, 1507–1510. [PubMed: 9626469]
- Mosesson Y, Mills GB, and Yarden Y (2008). Derailed endocytosis: an emerging feature of cancer. *Nat. Rev. Cancer* 8, 835–850. [PubMed: 18948996]
- Ohlstein B, and Spradling A (2006). The adult *Drosophila* posterior midgut is maintained by pluripotent stem cells. *Nature* 439, 470–474. [PubMed: 16340960]
- Ohlstein B, and Spradling A (2007). Multipotent *Drosophila* intestinal stem cells specify daughter cell fates by differential notch signaling. *Science* 315, 988–992. [PubMed: 17303754]
- Perez-Hernandez D, Gutiérrez-Vázquez C, Jorge I, López-Martín S, Ursa A, Sánchez-Madrid F, Vázquez J, and Yáñez-Mo M (2013). The intracellular interactome of tetraspanin-enriched microdomains reveals their function as sorting machineries toward exosomes. *J. Biol. Chem* 288, 11649–11661. [PubMed: 23463506]
- Pols MS, and Klumperman J (2009). Trafficking and function of the tetraspanin CD63. *Exp. Cell Res* 315, 1584–1592. [PubMed: 18930046]
- Port F, Chen HM, Lee T, and Bullock SL (2014). Optimized CRISPR/Cas tools for efficient germline and somatic genome engineering in *Drosophila*. *Proc. Natl. Acad. Sci. USA* 111, E2967–E2976. [PubMed: 25002478]
- Powell AE, Wang Y, Li Y, Poulin EJ, Means AL, Washington MK, Higginbotham JN, Juchheim A, Prasad N, Levy SE, et al. (2012). The pan-ErbB negative regulator Lrig1 is an intestinal stem cell marker that functions as a tumor suppressor. *Cell* 149, 146–158. [PubMed: 22464327]
- Rajesh S, Sridhar P, Tews BA, Fénéant L, Cocquerel L, Ward DG, Berditchevski F, and Overduin M (2012). Structural basis of ligand interactions of the large extracellular domain of tetraspanin CD81. *J. Virol* 86, 9606–9616. [PubMed: 22740401]
- Ren C, Finkel SE, and Tower J (2009). Conditional inhibition of autophagy genes in adult *Drosophila* impairs immunity without compromising longevity. *Exp. Gerontol* 44, 228–235. [PubMed: 18955126]
- Ren F, Wang B, Yue T, Yun E-Y, Ip YT, and Jiang J (2010). Hippo signaling regulates *Drosophila* intestine stem cell proliferation through multiple pathways. *Proc. Natl. Acad. Sci. USA* 107, 21064–21069. [PubMed: 21078993]
- Ren W, Zhang Y, Li M, Wu L, Wang G, Baeg GH, You J, Li Z, and Lin X (2015). Windpipe controls *Drosophila* intestinal homeostasis by regulating JAK/STAT pathway via promoting receptor endocytosis and lysosomal degradation. *PLoS Genet* 11, e1005180. [PubMed: 25923769]
- Rera M, Clark RI, and Walker DW (2012). Intestinal barrier dysfunction links metabolic and inflammatory markers of aging to death in *Drosophila*. *Proc. Natl. Acad. Sci. USA* 109, 21528–21533. [PubMed: 23236133]
- Resende LP, Truong ME, Gomez A, and Jones DL (2017). Intestinal stem cell ablation reveals differential requirements for survival in response to chemical challenge. *Dev. Biol* 424, 10–17. [PubMed: 28104389]
- Resnik-Docampo M, Koehler CL, Clark RI, Schinaman JM, Sauer V, Wong DM, Lewis S, D'Alterio C, Walker DW, and Jones DL (2017). Tricellular junctions regulate intestinal stem cell behaviour to maintain homeostasis. *Nat. Cell Biol* 19, 52–59. [PubMed: 27992405]
- Riedel F, Gillingham AK, Rosa-Ferreira C, Galindo A, and Munro S (2016). An antibody toolkit for the study of membrane traffic in *Drosophila melanogaster*. *Biol. Open* 5, 987–992. [PubMed: 27256406]
- Schindelin J, Arganda-Carreras I, Frise E, Kaynig V, Longair M, Pietzsch T, Preibisch S, Rueden C, Saalfeld S, Schmid B, et al. (2012). Fiji: an open-source platform for biological-image analysis. *Nat. Methods* 9, 676–682. [PubMed: 22743772]
- Shaw RL, Kohlmaier A, Polesello C, Veelken C, Edgar BA, and Tapon N (2010). The Hippo pathway regulates intestinal stem cell proliferation during *Drosophila* adult midgut regeneration. *Development* 137, 4147–4158. [PubMed: 21068063]
- Shravage BV, Hill JH, Powers CM, Wu L, and Baehrecke EH (2013). Atg6 is required for multiple vesicle trafficking pathways and hematopoiesis in *Drosophila*. *Development* 140, 1321–1329. [PubMed: 23406899]

- Song X, Zhu CH, Doan C, and Xie T (2002). Germline stem cells anchored by adherens junctions in the *Drosophila* ovary niches. *Science* 296, 1855–1857. [PubMed: 12052957]
- Staley BK, and Irvine KD (2010). Warts and Yorkie mediate intestinal regeneration by influencing stem cell proliferation. *Curr. Biol* 20, 1580–1587. [PubMed: 20727758]
- Sun S, and Irvine KD (2016). Cellular organization and cytoskeletal regulation of the Hippo signaling network. *Trends Cell Biol* 26, 694–704. [PubMed: 27268910]
- Thomas A, Lee PJ, Dalton JE, Nomie KJ, Stoica L, Costa-Mattioli M, Chang P, Nuzhdin S, Arbeitman MN, and Dierick HA (2012). A versatile method for cell-specific profiling of translated mRNAs in *Drosophila*. *PLoS ONE* 7, e40276. [PubMed: 22792260]
- Uchida S, Shimada Y, Watanabe G, Li ZG, Hong T, Miyake M, and Imamura M (1999). Motility-related protein (MRP-1/CD9) and KAI1/CD82 expression inversely correlate with lymph node metastasis in oesophageal squamous cell carcinoma. *Br. J. Cancer* 79, 1168–1173. [PubMed: 10098753]
- Vani K, Yang G, and Mohler J (1997). Isolation and cloning of a *Drosophila* homolog to the mammalian RACK1 gene, implicated in PKC-mediated signalling. *Biochim. Biophys. Acta* 1358, 67–71. [PubMed: 9296523]
- Wei X, and Ellis HM (2001). Localization of the *Drosophila* MAGUK protein Polychaetoid is controlled by alternative splicing. *Mech. Dev* 100, 217–231. [PubMed: 11165479]
- Wu VM, Schulte J, Hirschi A, Tepass U, and Beitel GJ (2004). Sinuous is a *Drosophila* claudin required for septate junction organization and epithelial tube size control. *J. Cell Biol* 164, 313–323. [PubMed: 14734539]
- Xu H, Lee SJ, Suzuki E, Dugan KD, Stoddard A, Li HS, Chodosh LA, and Montell C (2004). A lysosomal tetraspanin associated with retinal degeneration identified via a genome-wide screen. *EMBO J* 23, 811–822. [PubMed: 14963491]
- Xu C, Ericsson M, and Perrimon N (2018). Understanding cellular signaling and systems biology with precision: a perspective from ultrastructural and organelle studies in the *Drosophila* midgut. *Curr. Opin. Syst. Biol* 11, 24–31.
- Yoo TH, Ryu BK, Lee MG, and Chi SG (2013). CD81 is a candidate tumor suppressor gene in human gastric cancer. *Cell Oncol. (Dordr.)* 36, 141–153. [PubMed: 23264205]
- Zeng X, Chauhan C, and Hou SX (2010). Characterization of midgut stem cell- and enteroblast-specific Gal4 lines in *Drosophila*. *Genesis* 48, 607–611. [PubMed: 20681020]
- Zhang XA, Bontrager AL, and Hemler ME (2001). Transmembrane-4 superfamily proteins associate with activated protein kinase C (PKC) and link PKC to specific beta(1) integrins. *J. Biol. Chem* 276, 25005–25013. [PubMed: 11325968]
- Zhang J, Niu C, Ye L, Huang H, He X, Tong WG, Ross J, Haug J, Johnson T, Feng JQ, et al. (2003). Identification of the haematopoietic stem cell niche and control of the niche size. *Nature* 425, 836–841. [PubMed: 14574412]
- Zhang J, Schulze KL, Hiesinger PR, Suyama K, Wang S, Fish M, Acar M, Hoskins RA, Bellen HJ, and Scott MP (2007). Thirty-one flavors of *Drosophila* rab proteins. *Genetics* 176, 1307–1322. [PubMed: 17409086]
- Zhao B, Ye X, Yu J, Li L, Li W, Li S, Yu J, Lin JD, Wang CY, Chinnaiyan AM, et al. (2008). TEAD mediates YAP-dependent gene induction and growth control. *Genes Dev* 22, 1962–1971. [PubMed: 18579750]
- Zihni C, Mills C, Matter K, and Balda MS (2016). Tight junctions: from simple barriers to multifunctional molecular gates. *Nat. Rev. Mol. Cell Biol* 17, 564–580. [PubMed: 27353478]
- Zimmerman B, Kelly B, McMillan BJ, Seegar TCM, Dror RO, Kruse AC, and Blacklow SC (2016). Crystal structure of a full-length human Tetraspanin reveals a cholesterol-binding pocket. *Cell* 167, 1041–1051.e1011. [PubMed: 27881302]

Highlights

- The assembly of septate junctions (SJs) occurs during ISC-EC differentiation
- The SJ protein Tsp2A undergoes internalization and mediates aPKC degradation
- Normal Tsp2A-SJ assembly ensures Hippo signaling to restrict ISC proliferation
- Defective Tsp2A-SJ assembly causes aPKC accumulation and Yki hyperactivity

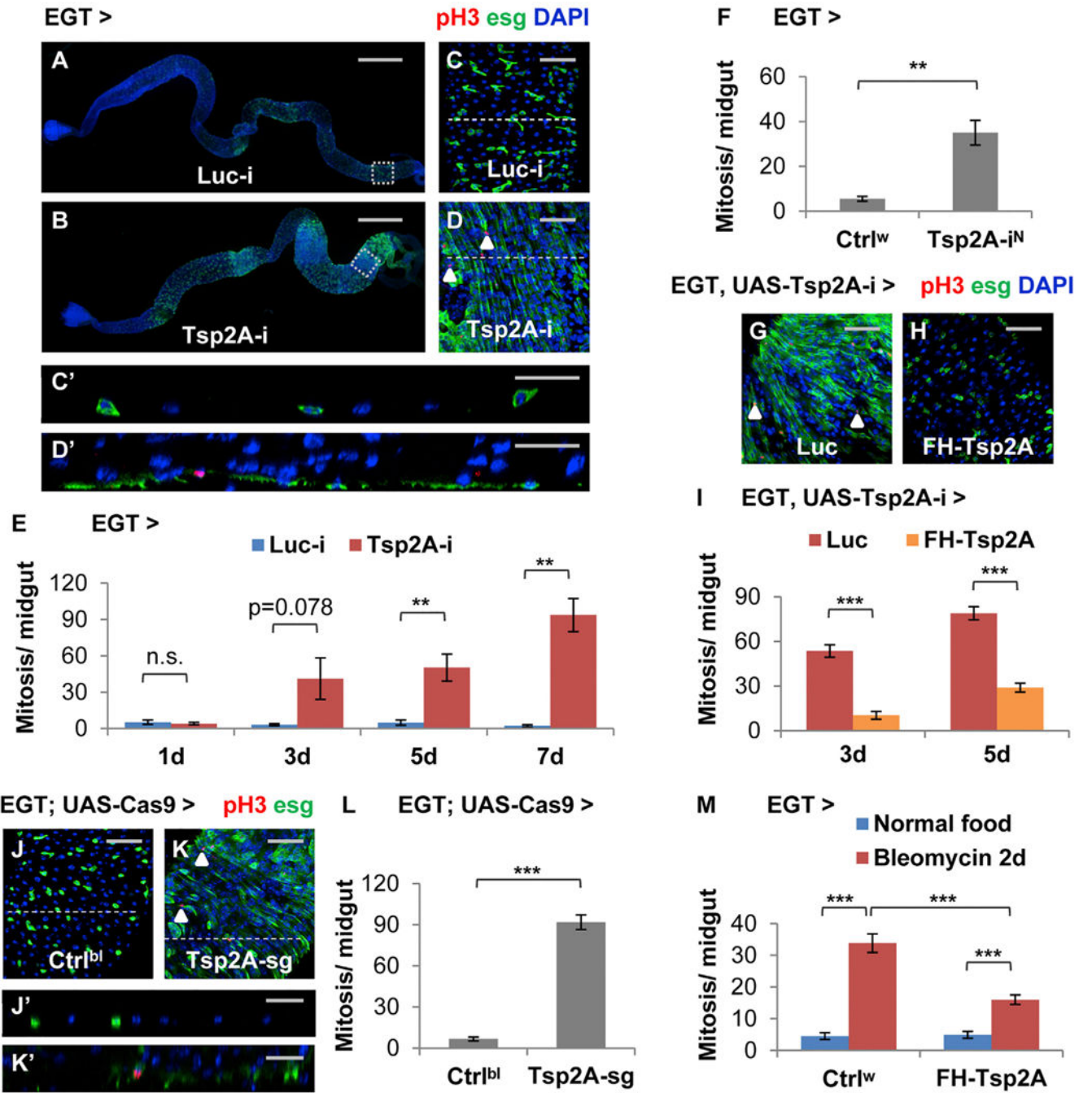


Figure 1. Identification of *Tsp2A* as a Suppressor of Proliferation in ISCs/EBs
 (A and B) Images showing the entire midgut with *Luciferase (Luc)* RNAi (the negative control) (A) or *Tsp2A* RNAi (B) expression in ISCs/EBs for 5 days. Scale bar, 500 mm. The GFP signal under the control of *EGT* labels ISCs/EBs and their recent progenies due to signal perdurance.
 (C and D) The midgut expressing *Luc* RNAi or *Tsp2A* RNAi in ISCs/EBs for 5d were stained for the mitosis marker phospho-histone H3 (pH3). Scale bar, 50 μ m. Examples of

pH3⁺ cells were labeled with white arrowheads. (C) and (D) correspond to the posterior midgut regions encircled with white dashed squares in (A) and (B), respectively.

(C' and D') The orthogonal projection images showing the cross-sections indicated by dashed lines in (C) and (D), respectively. Scale bar, 25 μ m.

(E) Mitosis quantification of midguts expressing *Luc* RNAi or *Tsp2A* RNAi in ISCs/EBs for 1, 3, 5, or 7 days. For each genotype at each time point, at least 6 midguts were analyzed.

Data are represented as mean \pm SEM.

(F) Mitosis quantification of midguts expressing a different *Tsp2A* RNAi (from NIG, with superscript label 'N') in ISCs/EBs for 7 days. Ctrl^w (genotype: *w1118*) was used in genetic crosses as the control, because the genetic background is the same as NIG stocks. N = 7 or 6 midguts were analyzed for the genotype group of Ctrl^w or *Tsp2A-i^N*, respectively. Data are represented as mean \pm SEM.

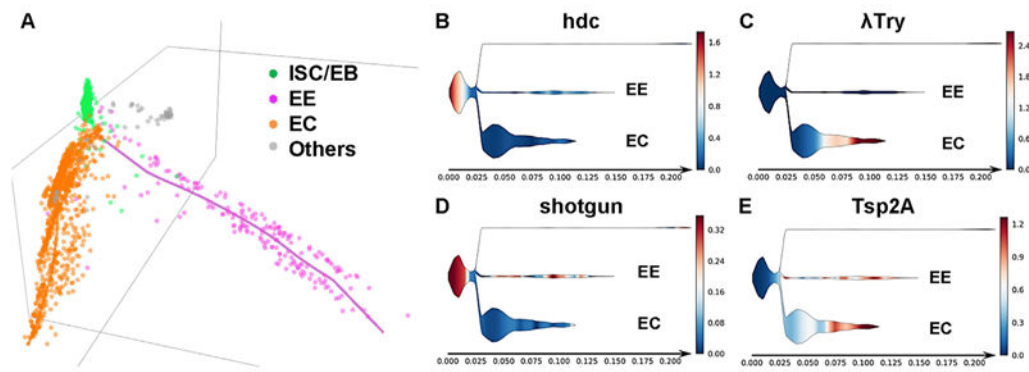
(G and H) pH3 staining of midguts expressing *Tsp2A* RNAi together with *Luc* cDNA (G) or *FH-Tsp2A* (H) in ISCs/EBs for 5 days. Scale bar, 50 μ m. *FH-Tsp2A* is resistant to the knockdown of *Tsp2A* RNAi (the Bloomington stock), which targets the 3' UTR region of *Tsp2A*. White arrowheads highlight examples of pH3⁺ cells.

(I) Mitosis quantification of midguts expressing *Tsp2A* RNAi together with *Luc* cDNA or *FH-Tsp2A* in ISCs/EBs for 3 or 5 days. N > 12 midguts were analyzed for each group. Data are represented as mean \pm SEM.

(J–L) pH3 staining (K) and mitosis quantification (L) of midguts with ubiquitous expression of sgRNAs against *Tsp2A* and targeted expression of *Cas9* in ISCs/EBs for 7 days. Scale bar, 50 μ m. Flies with the same genetic background but only empty insertional landing sites (*y v; atp2*) were used as the control (Ctrl^{bl}) (J) for sgRNA. White arrowheads highlight examples of pH3⁺ cells. N = 10 midguts were analyzed per genotype for quantification. Data are represented as mean \pm SEM.

(J' and K') The orthogonal projection images showing the cross sections indicated by dashed lines in (G) and (H), respectively. Scale bar, 25 μ m.

(M) Mitosis quantification of midguts with or without *FH-Tsp2A* expression in ISCs/EBs for 5 days, with or without bleomycin feeding for the last 2 days before dissection. Ctrl^w flies were used as the control in genetic crosses for *FH-Tsp2A* overexpression. N = 12 midguts were analyzed for each group. Data are represented as mean \pm SEM.



F Tsp2A co-expression analysis

Cell type markers	esg+	DI+	klu+	Myo1A+	βTry+	λTry+
Total number captured	333	84	105	199	648	348
Tsp2A+ cell number	18	5	15	93	188	139
Tsp2A+ cell percentage	5.41%	5.95%	14.29%	46.73%	29.01%	39.94%
Average Tsp2A expression	0.103	0.117	0.254	0.804	0.522	0.799

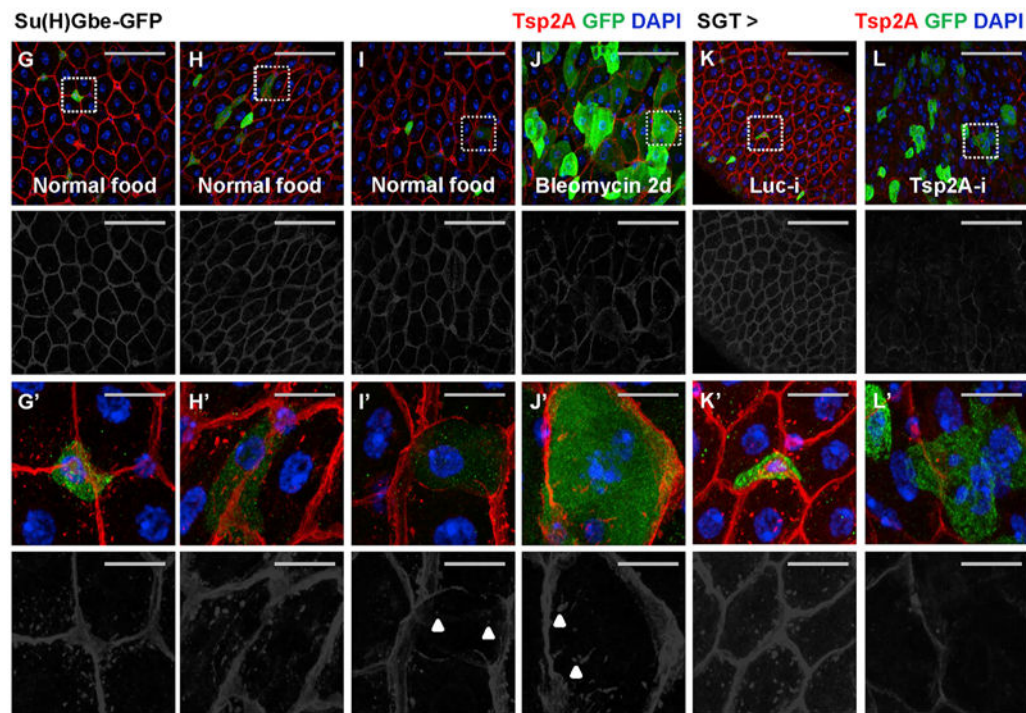


Figure 2. *Tsp2A* Expression Initiates in ISCs and Increases during ISC-EC Differentiation

(A) STREAM analysis of single-cell RNA-seq reconstructs the trajectories of ISC differentiation toward the EE and EC lineages (Hung et al., 2018). Each dot in the 3D scattered plot represents a cell. The colored axes represent pseudotime for temporal trajectories. The different cell types (ISC/EB in green, EE in pink, EC in orange, and others in gray) were recognized by unsupervised clustering and the expression of known marker genes. The cell population at the distal end of EC differentiation is expected to be

underrepresented in our analysis, because the large and presumably more mature ECs are likely to be filtered out when we used a 25 μm cell strainer to obtain dissociated single cells. (B–E) STREAM plots in 2D projection map the expression of *hdc* (B), *λ -Trypsin* (C), *shotgun* (D), and *Tsp2A* (E) during ISC differentiation. The x axis indicates the hypothetical time in differentiation. The branch width in the y axis indicates the number of cells at a particular pseudotime in the branch. The ISCs/EBs are positioned on the left. The branches of EEs and ECs are positioned on the right. Other non-epithelial cells in the gut, shown in the top branch of each panel, are not derived from ISCs and thus barely connected to the rest of the plot. The color gradient scale bar indicating normalized expression levels (blue means low and red means high) is attached to the right of each panel.

(F) *Tsp2A* co-expression analysis based on single-cell RNA-seq (Table S1). We counted the number of cells expressing different cell markers and cells expressing *Tsp2A* together with each marker. The percentage of *Tsp2A*⁺ cells and the average normalized *Tsp2A* expression levels in each population sorted by these markers are also listed in the summary chart.

(G–J) Midguts from young adult flies fed with normal food (G–I) or bleomycin (J) for 2 days were co-stained for Tsp2A and the EB marker Su(H)Gbe-GFP. Scale bar, 50 μm . The red channel of Tsp2A staining signals is presented in grayscale below each of the merged images.

(G'–J') High-magnification images, corresponding to the regions encircled with white dashed squares in G–J, exhibit different levels (G', no expression; H', weak; I', medium; J', strong) of Tsp2A expression in EBs. Scale bar, 10 μm .

(K and L) Tsp2A staining of midguts expressing *Luc* RNAi (K) or *Tsp2A* RNAi (L) in EBs with *SGT* driver for 7 days. *SGT*-driven *GFP* expression labels EBs. A zoom-in view of encircled regions is shown in (K' and L').

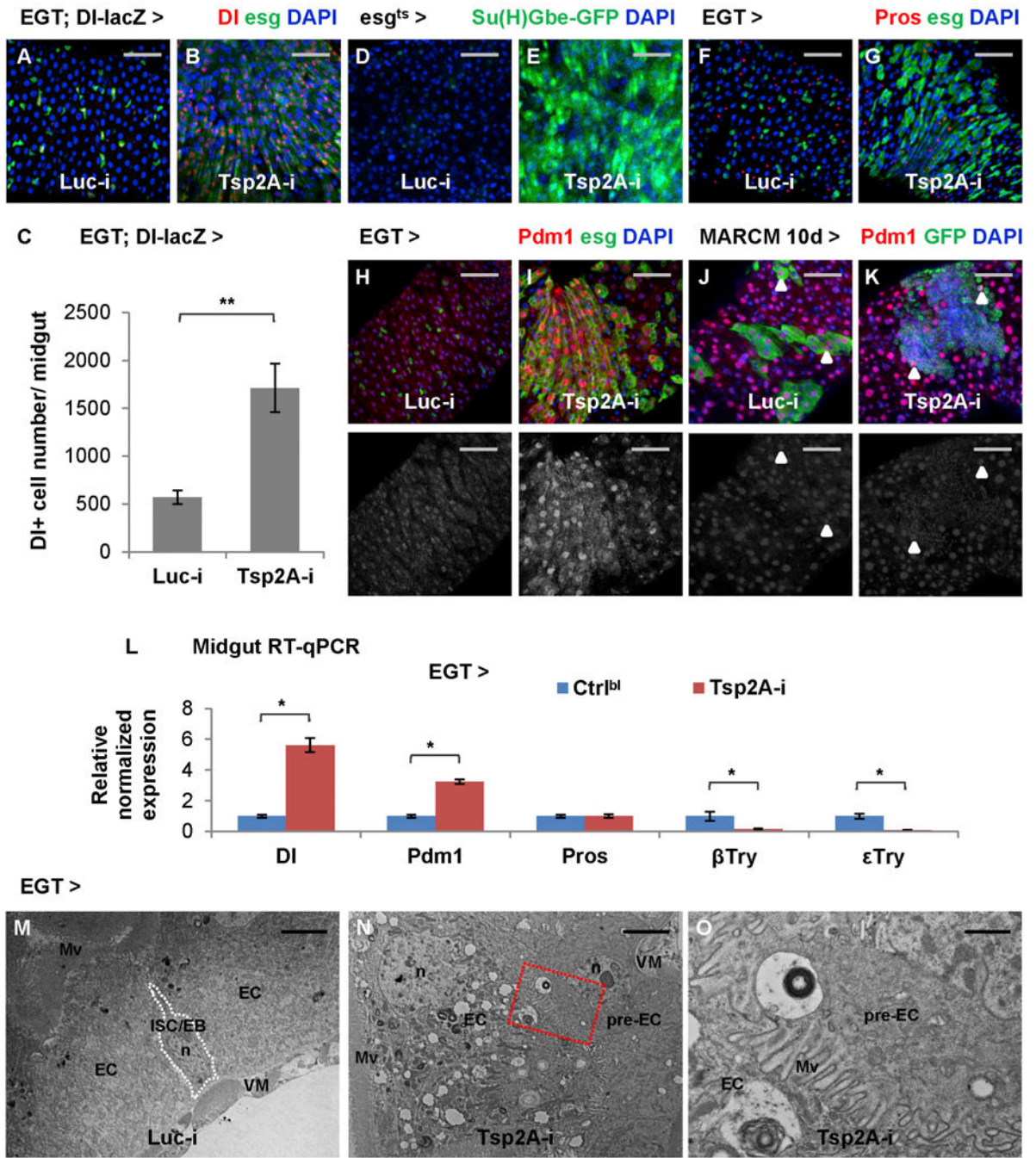


Figure 3. *Tsp2A* Knockdown Results in the Accumulation of ISCs/EBs and Pre-ECs
 (A and B) Midguts expressing *Luc* RNAi (A) or *Tsp2A* RNAi (B) in ISCs/EBs for 3 days are stained for the ISC marker DI-lacZ. Scale bar, 50 μm.
 (C) Quantification of DI+ cells in the midguts expressing *Luc* RNAi or *Tsp2A* RNAi in ISCs/EBs for 5d. N > 8 midguts were analyzed for each group. Data are represented as mean ± SEM.
 (D–I) Midguts expressing *Luc* RNAi (D, F, and H) or *Tsp2A* RNAi (E, G, and I) in ISCs/EBs (driven by *EGT* or *tubGal80^{ts}; esgGal4 (esgGal4^{ts})*) for 3 days are stained for the

EB marker/Notch pathway reporter Su(H)Gbe-GFP (D and E), the EE marker Pros (F and G), or the EC marker Pdm1 (H and I). Scale bar, 50 μm . The red channel of Pdm1 signals is presented in grayscale below each of the merged images.

(J and K) Pdm1 staining of midgut with MARCM clones induced to express *Luc* RNAi (J) or *Tsp2A* RNAi (K) for 10 days. Scale bar, 50 μm . Arrowheads highlight examples of polyploid ECs in the lineage of randomly labeled ISCs that express *Luc* RNAi or *Tsp2A* RNAi. In the MARCM clone expressing *Tsp2A* RNAi, even the small nuclei are mostly stained positive for Pdm1.

(L) qRT-PCR quantification of midguts expressing *Tsp2A* RNAi in ISCs/EBs for 7 days for the different cell-type markers *Dl*, *Pdm1*, *Pros*, β -*Trypsin*, and *e-Trypsin*. Data are represented as mean \pm SEM.

(M and N) Electron micrographs of midguts expressing *Luc* RNAi (M) or *Tsp2A* RNAi (N) in ISCs/EBs for 5 days. Scale bar, 4 μm . Pre-ECs are the progenitor cells differentiating toward ECs, which exhibit mixed features of ISCs/EBs and ECs. Mv, microvilli; n, nucleus; VM, visceral muscle.

(O) A zoomed-in view of the region encircled with the red dashed box in (N) shows the formation of microvilli at the apical surface of a basally localized pre-EC. Scale bar, 1 μm .

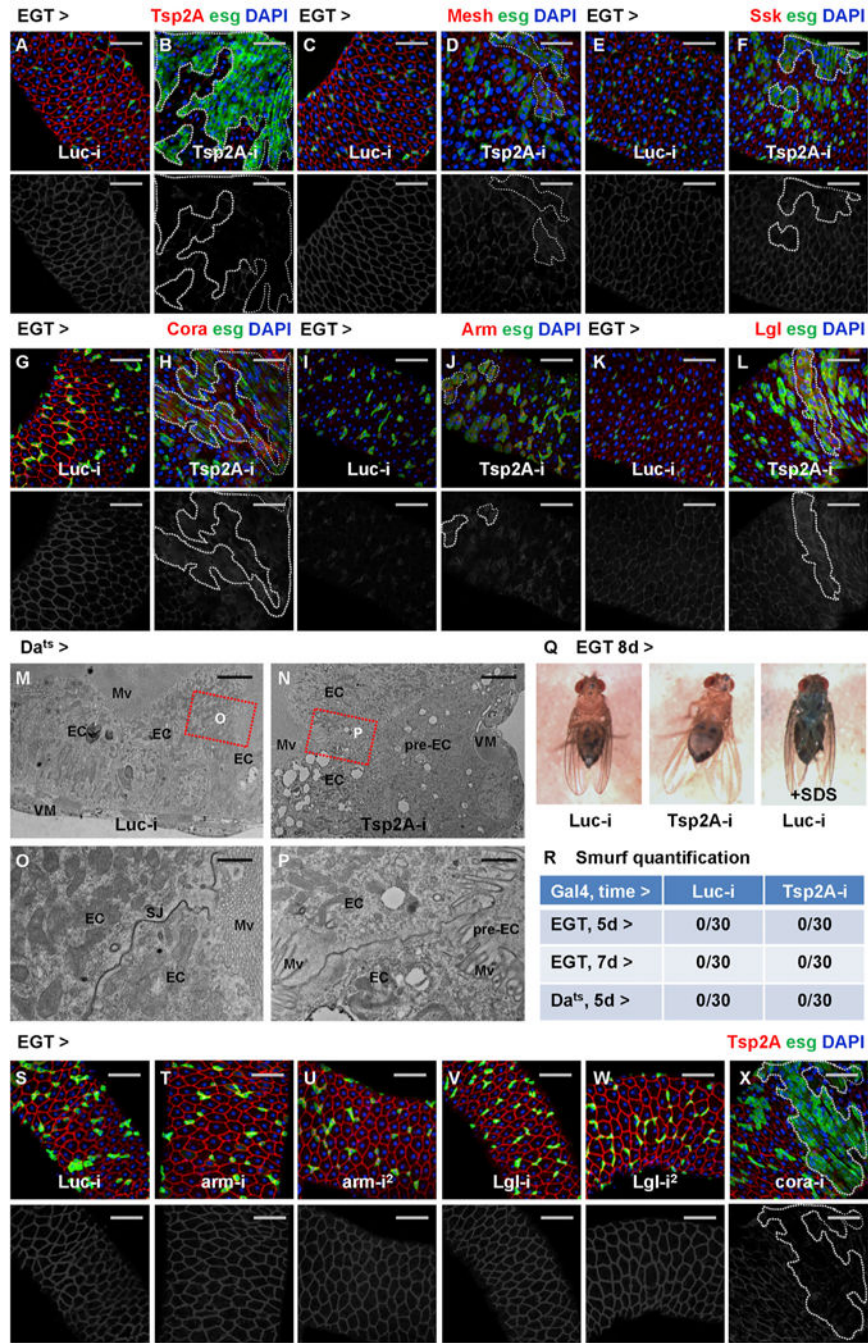


Figure 4. SJ Proteins Are Interdependent and Distinct from Other Junctions for Their Membrane Localization in the Midgut Epithelium
 (A–L) Midguts expressing *Luc* RNAi (A, C, E, G, I, and K) or *Tsp2A* RNAi (B, D, F, H, J, and L) in ISCs/EBs for 3 days are stained for different junction proteins: Tsp2A (A and B), Mesh (C and D), Ssk (E and F), Cora (G and H), Arm (I and J), and Lgl (K and L). Scale bar, 50 μ m. Dashed lines circle example regions (GFP+ ISCs/EBs and recent progenies due to perdurance) where *Tsp2A* RNAi is expressed. The red channel is presented in grayscale below each of the merged images (in A–L and S–X). Note that ISC tumors often initiate sporadically from a few ISCs/EBs expressing *Tsp2A* RNAi (Figures 4D, 4F, 4H, 4J, and

4L), which probably correspond to the relatively infrequent events of ISC-EC differentiation under normal feeding conditions.

(M and N) Electron micrographs of midguts ubiquitously expressing *Luc* RNAi (M) or *Tsp2A* RNAi (N) for 5 days. Scale bar, 4 μ m.

(O and P) High-magnification images of midguts ubiquitously expressing *Luc* RNAi (O) or *Tsp2A* RNAi (P), corresponding to regions encircled with red dashed boxes in (M) or (N), show the cell junctions between ECs. Scale bar, 1 μ m.

(Q) Smurf assay to evaluate the barrier function of midguts expressing *Luc* RNAi or *Tsp2A* RNAi in ISCs/EBs for 8 days. Flies fed with 1% SDS are used as a positive control. Note that although *Tsp2A* knockdown does not affect barrier function in young adult flies, prolonged RNAi expression (for more than 10 days; data not shown) could cause gut leakage in old flies.

(R) Quantification of Smurf-positive (leaky) flies among assayed flies expressing *Luc* RNAi or *Tsp2A* RNAi in ISCs/EBs or ubiquitously for 5–7 days. N = 30 flies are analyzed for each genotype at each time point.

(S–X) Tsp2A staining of midguts expressing *Luc* RNAi (S), *arm* RNAi (T and U, two different lines), *Lg1* RNAi (V and W, two different lines), or *cora* RNAi (X) in ISCs/EBs. Scale bar, 50 μ m. All RNAi lines are expressed for 7 days, except *cora* RNAi, for which expression for 3 days is sufficient to cause overproliferation and disrupt Tsp2A expression.

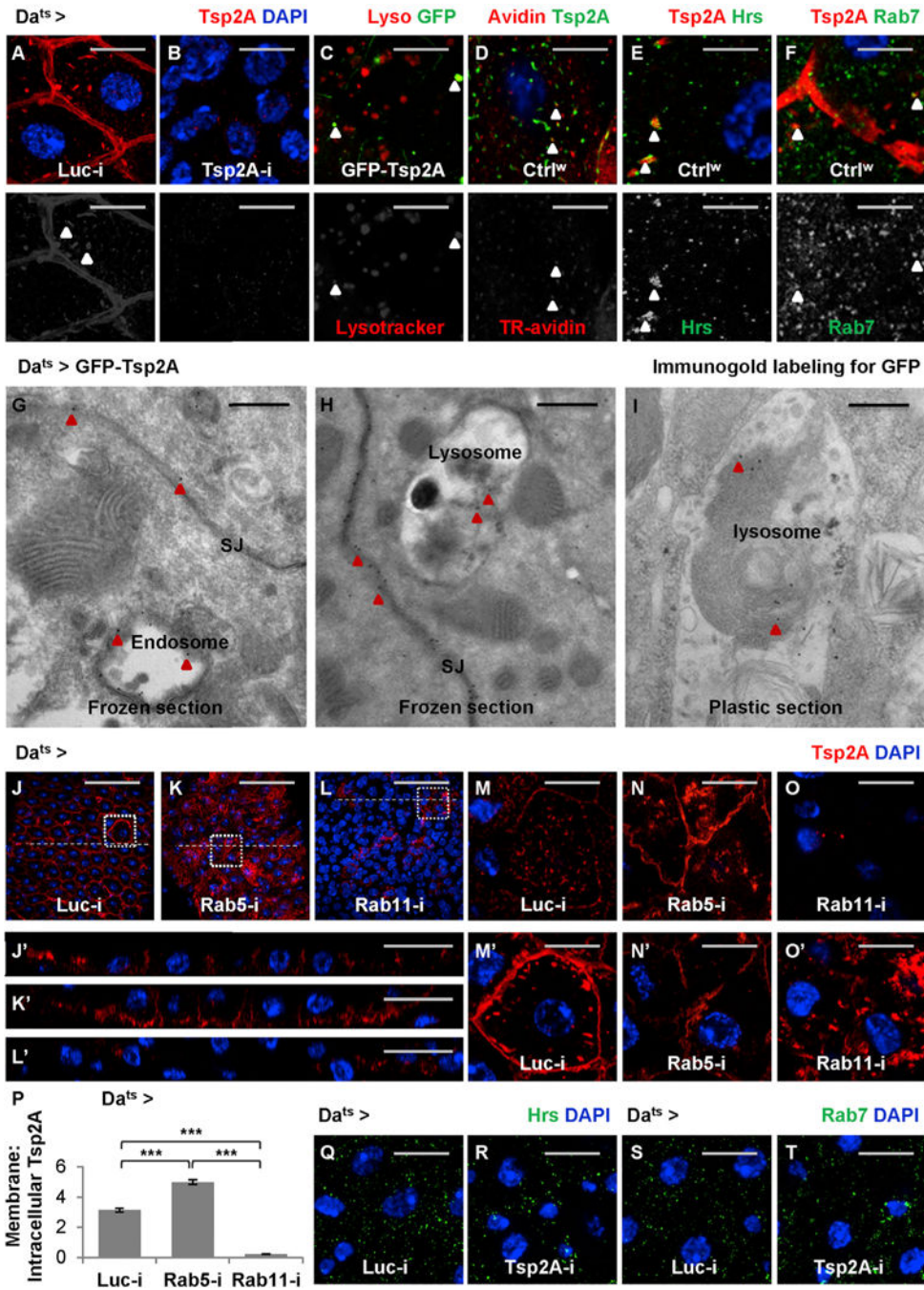


Figure 5. Tsp2A Participates in the Endocytic Cycle

(A and B) Midguts expressing *Luc* RNAi (A) or *Tsp2A* RNAi (B) ubiquitously for 3 days are stained for Tsp2A. Scale bar, 10 μ m. The Tsp2A staining found in intracellular punctae is not background noise, because it can be eliminated by *Tsp2A* knockdown. The red channel is presented in grayscale below the merged images (in A–D).

(C) Midguts ubiquitously expressing *GFP-Tsp2A* for 5 days are stained with LysoTracker red to label lysosomes or other acidic compartments. Scale bar, 10 μ m. Arrowheads indicate the co-localization of GFP-labeled Tsp2A with LysoTracker. To avoid potential co-

localization artifacts caused by overlaying different focal planes, a single z stack of confocal image is presented.

(D) Endocytosis assay. Wild-type midguts incubated with Texas-red-labeled avidin (TR-avidin) for 20 min are fixed and stained for Tsp2A. Scale bar, 5 μ m. Arrowheads indicate Tsp2A punctae co-localization with internalized TR-avidin. A single z stack image (close to the cell surface) is presented. (E and F) Wild-type midguts are co-stained for Tsp2A and the early endosome marker Hrs (E) or the late endosome marker Rab7 (F). Scale bar, 5 μ m. Arrowheads indicate Tsp2A punctae co-localization with Hrs or Rab7. Single z stack images are presented. The green channels are presented in grayscale below the merged images. (G and H) Immunogold labeling and electron micrographs of frozen sections from midguts ubiquitously expressing *GFP-Tsp2A* for 5 days. Scale bar, 400 nm. Red arrowheads indicate examples of the 15 nm gold (black dots) labeling GFP-Tsp2A found in SJs (G and H), endosome (G), and lysosome (H).

(I) Immunoelectron microscopy (immuno-EM) of the plastic-embedded midgut section showing gold labeled GFP-Tsp2A (indicated by red arrowheads) in the lysosome. Scale bar, 400 nm. Compared to frozen sections, plastic sections perform better in maintaining the GFP antigen in lysosomes for immuno-EM.

(J–L) Tsp2A staining of midguts ubiquitously expressing *Luc* RNAi (J), *Rab5* RNAi (K), or *Rab11* RNAi (L) for 5 days. Scale bar, 50 μ m.

(J'–L') The orthogonal projection images showing the cross-sections indicated by dashed lines in J–L. Scale bar, 20 μ m.

(M–O) High-magnification, single z stack images near the cell surface of midguts ubiquitously expressing *Luc* RNAi (M), *Rab5* RNAi (N), or *Rab11* RNAi (O), corresponding to regions encircled with white dashed squares in J–L. Scale bar, 10 μ m.

(M'–O') High-magnification, single z stack images near the cell center, corresponding to regions encircled with white dashed squares in J–L. Scale bar, 10 μ m.

(P) Quantification of the ratios of membrane-localized to intracellular Tsp2A staining intensity in midguts ubiquitously expressing *Luc* RNAi, *Rab5* RNAi, or *Rab11* RNAi for 5 days. 24 cells from 3 midguts were analyzed for each genotype. Data are presented as mean \pm SEM.

(Q–T) Hrs (Q and R) or Rab7 (S and T) staining of midguts expressing *Luc* RNAi (Q and S) or *Tsp2A* RNAi (R and T) ubiquitously for 3 days. Scale bar, 10 μ m.

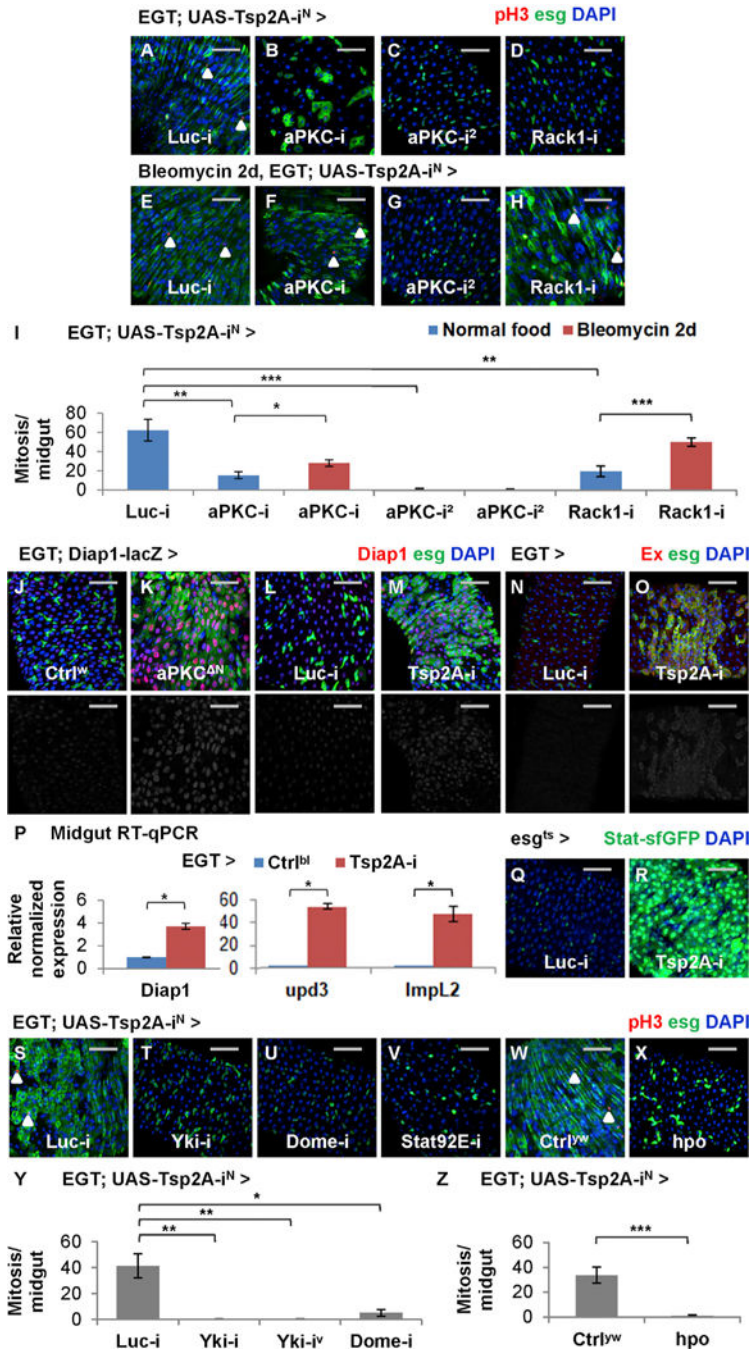


Figure 6. aPKC Is Required for *Tsp2A* RNAi-Induced Overproliferation and Couples *Tsp2A* Knockdown with Yki and JAK-Stat Signaling
 (A–H) pH3 staining of midguts expressing *Tsp2A* RNAi together with *Luc* RNAi (A and E), *aPKC* RNAi (B, C, F, and G, two different lines), or *Rack1* RNAi (D and H) in ISC/EBs for 5 days, with (E–H) or without (A–D) additional 2-day feeding with bleomycin. Scale bar, 50 μ m. White arrowheads highlight examples of pH3+ cells.
 (I) Mitosis quantification of midguts expressing *Tsp2A* RNAi together with *Luc* RNAi, *aPKC* RNAi, or *Rack1* RNAi in ISC/EBs for 7 days, with or without the last 2-day feeding

with bleomycin. $N > 7$ midguts are analyzed for each group. Data are represented as mean \pm SEM.

(J and K) Midguts with (K) or without (J) constitutively active *aPKC* (*aPKC^N*) expression in ISCs/EBs for 3 days are stained for the Yki reporter Diap1-lacZ. Scale bar, 50 μ m. The red channels are presented in grayscale, below the merged images.

(L and M) Midguts expressing *Luc* RNAi (L) or *Tsp2A* RNAi (M) in ISCs/EBs for 3 days are stained for Diap1-lacZ. Scale bar, 50 μ m.

(N and O) Midguts expressing *Luc* RNAi (N) or *Tsp2A* RNAi (O) in ISCs/EBs for 3 days are stained for Ex, a transcriptional target of Yki. Scale bar, 50 μ m.

(P) qRT-PCR measurement of Yki responsive genes (*Diap1*, *upd3*, and *ImpL2*) in midguts with or without *Tsp2A* RNAi expression in ISCs/EBs for 7 days. Data are represented as mean \pm SEM.

(Q and R) Midguts expressing *Luc* RNAi (Q) or *Tsp2A* RNAi (R) in ISCs/EBs (driven by *esg^{ts}*) for 3 days are stained for the JAK-Stat pathway reporter Stat-sfGFP. Scale bar, 50 μ m.

(S–V) pH3 staining of midguts expressing *Tsp2A* RNAi together with *Luc* RNAi (S), *Yki* RNAi (T), *Dome* RNAi (U), or *Stat92E* RNAi (V) in ISCs/EBs for 5 days. Scale bar, 50 μ m.

(W and X) pH3 staining of midguts expressing *Tsp2A* RNAi alone (W) or *Tsp2A* RNAi together with *hpo* (X) in ISCs/EBs for 5 days. Scale bar, 50 μ m. Ctrl^{y^w} (genotype: *y w*) flies have the same genetic background as the *UAS-hpo* line. White arrowheads highlight examples of pH3+ cells.

(Y) Mitosis quantification of midguts expressing *Tsp2A* RNAi together with *Luc* RNAi, *Yki* RNAi (two different lines), or *Dome* RNAi for 5 days. $N > 5$ midguts are analyzed for each group. Data are represented as mean \pm SEM.

(Z) Mitosis quantification of midguts expressing *Tsp2A* RNAi alone or together with *hpo* in ISCs/EBs for 5 days. $N > 7$ midguts are analyzed for each group. Data are represented as mean \pm SEM.

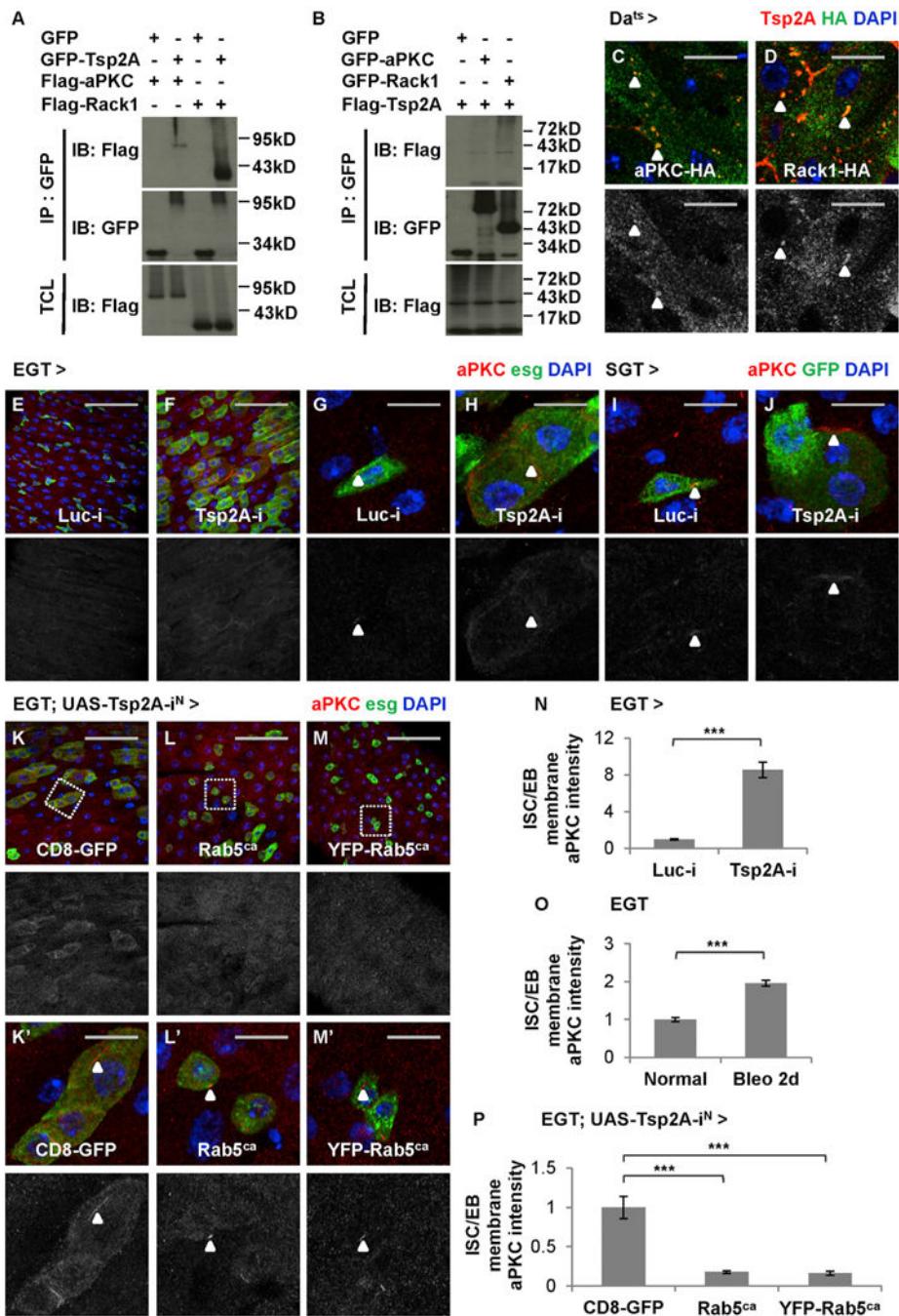


Figure 7. Tsp2A Functions as an Adaptor Facilitating aPKC/Rack Degradation

(A and B) S2R+ cell extracts expressing GFP or GFP fusion proteins are subjected to immunoprecipitation with GFP-Trap beads. IB, immunoblot; IP, immunoprecipitation; TCL, total cell lysate. GFP-Tsp2A co-precipitates with FLAG-aPKC and FLAG-Rack1 (A), whereas both GFP-aPKC and GFP-Rack1 co-precipitate with FLAG-Tsp2A (B). Note that the expected size of Tsp2A (without any tag) is 26.9 kDa and that the bands larger (appear as smears) or smaller than expected could represent modified or degraded forms of Tsp2A, according to a previous report (Izumi et al., 2016).

(C and D) Midguts expressing HA-tagged *aPKC-HA* (C) or *Rack1-HA* (D) are co-stained with anti-Tsp2A and anti-HA antibodies. Scale bar, 10 μ m. Single z stack images are presented. The green channels of HA staining are presented in grayscale below the merged images. Arrowheads indicate examples of aPKC or Rack1 co-localization with Tsp2A punctae.

(E–H) Regular (E and F; scale bar, 50 μ m) or high-magnification (G and H; scale bar, 10 μ m) confocal images showing aPKC staining of midguts expressing *Luc* RNAi (E and G) or *Tsp2A* RNAi (F and H) in ISCs/EBs for 3 days. The red channels are presented in grayscale below the merged images (in E–M and K'–M'). Arrowheads highlight examples of membrane-localized aPKC staining.

(I and J) High-magnification images showing aPKC staining of midguts expressing *Luc* RNAi (I) or *Tsp2A* RNAi (J) in EBs for 7 days. Scale bar, 10 μ m. Arrowheads indicate examples of concentrated aPKC staining.

(K–M) aPKC staining of midguts expressing *Tsp2A* RNAi together with *CD8-GFP* (control) (K) or *Rab5^{ca}* (2 different lines, with, M, or without, L, YFP tag) in ISCs/EBs for 5 days. Scale bar, 50 μ m.

(K'–M') High-magnification images of regions encircled with wash dashed squares in K–M. Scale bar, 10 μ m. Arrowheads indicate aPKC staining.

(N) Quantification of relative aPKC signal intensity on the membrane of ISCs/EBs expressing *Luc* RNAi or *Tsp2A* RNAi for 3 days. N = 32 cells from 4 midguts were analyzed for each genotype. Data are represented as mean \pm SEM.

(O) Quantification of relative aPKC staining intensity on the membrane of ISCs/EBs in midguts from young adult flies on normal food or on bleomycin food for 2 days before dissection. N = 30 cells from 3 midguts were analyzed for each group. Data are represented as mean \pm SEM.

(P) Quantification of relative aPKC signal intensity on the membrane of ISCs/EBs expressing *Tsp2A* RNAi together with *CD8-GFP*, *Rab5^{ca}*, or *YFP-Rab5^{ca}* for 5 days. N = 18 cells from 3 midguts were analyzed for each genotype. Data are represented as mean \pm SEM.